Precambrian Research 361 (2021) 106260

Contents lists available at ScienceDirect

Precambrian Research

journal homepage: www.elsevier.com/locate/precamres

Early Palaeoproterozoic granulite-facies metamorphism and partial melting of eclogite-facies rocks in the Salma association, eastern Fennoscandian Shield, Russia

Ksenia Dokukina [a,*], M.V. Mints [a], V.B. Khubanov [b], V.S. Sheshukov [a], A.N. Konilov [a,c], T. B. Bayanova [d], T.V. Kaulina [d], M.A. Golunova [b], P.A. Dokukin [e], O.I. Okina [a], K.V. Van [c], D. S. Yudin [f,g], A.V. Travin [f,g], A.V. Zaitsev [a], V.L. Kosorukov [h], V.I. Pozhilenko [d], T.I. Golovanova [i]

[a] Geological Institute of RAS, Moscow, Russia
[b] Geological Institute of SB RAS, Ulan-Ude, Russia
[c] Institute of Experimental Mineralogy, RAS, Chernogolovka, Russia
[d] Institute of Geology of the Kola Science Centre, RAS, Apatity, Russia
[e] Peoples' Friendship University of Russia, Moscow, Russia
[f] Sobolev V.S. Institute of Geology and Mineralogy SB RAS, Novosibirsk, Russia
[g] Novosibirsk State University, Russia
[h] Lomonosov Moscow State University, Russia
[i] Institute of Geology of Ore Deposits, Petrography, Mineralogy and Geochemistry RAS, Moscow, Russia

ARTICLE INFO

Keywords:
Metasedimentary rocks
Pillow lava
Eclogite
Granulite
Partial melting
U-Pb dating

ABSTRACT

The Salma-type Archaean eclogites exposed along the northwestern boundary of the Belomorian Eclogite Province in the eastern Fennoscandian Shield formed as a result of the Mesoarchaean–Neoarchaean subduction and collision. The common protoliths of the Salma-type subduction-related eclogites were oceanic layered gabbro and volcanic-sedimentary assemblage. The eclogite-facies pillow lavas and associated alumina-siliceous sediments that fill interpillow space and intercalate with lava flows are the main objects of our work. The kyanite-garnet–phengite–quartz rocks formed after alumina-siliceous sediments contain fluid inclusions trapped in large relic quartz grains. The fluid inclusions yielded an isochore that corresponds to PT-conditions of a beginning of the Salma oceanic rock subduction from the seafloor level that generally confirms the sedimentary provenance of these rocks. The alumina-siliceous sediments underwent the eclogite-facies metamorphism at pressure no lower than 21 kbar and temperatures of 650–750 °C and transformed into kyanite-garnet–phengite–quartz rocks. During exhumation under granulite-facies conditions at temperatures up to 900 °C and pressure down to 9 kbar, eclogite facies metasediments underwent partial melting accompanied by disequilibrium breakdown of phengite + quartz association with formation complex polymineralic pseudomorphs consisting of feldspars, biotite, muscovite, kyanite, corundum, and dumortierite. U-Pb dating of Th-rich igneous zircon from melted metasedimentary and mafic rocks using the LA-ICP-MS and TIMS methods yielded the time of granulite facies event accompanied by partial melting processes at ~2.45 Ga. After this, zircon underwent fluid-induced alteration, causing partial dissolution followed by precipitation of new Th–poor zircon and zircon rims around ancient grains at ~1.9 Ga ago

1. Introduction

In recent decades, the Mesoarchaean–Neoarchaean Belomorian Eclogite Province (Fig. 1) was discovered in the eastern Fennoscandia Shield (Kola-Karelia region) (Volodichev et al., 2004; Mints et al., 2010) and then thoroughly studied by several scientific teams (Dokukina et al., 2012, 2014, 2017; Dokukina, 2017; Dokukina and Mints, 2019; Kaulina et al., 2010; Li et al., 2017a,b; Liu et al., 2017; Mints et al., 2014; Mints and Dokukina, 2020a,b; Perchuk and Morgunova, 2014; Shchipansky et al., 2012a,b; Skublov et al., 2011a,b, 2012; Slabunov et al., 2011b;

* Corresponding author.
E-mail address: ksdokukina@gmail.com (K. Dokukina).

https://doi.org/10.1016/j.precamres.2021.106260
Received 8 June 2020; Received in revised form 29 April 2021; Accepted 30 April 2021

Volodichev et al., 2012; Dokukina and Konilov, 2011; Dokukina et al., 2015; Dokukina et al., 2020; Konilov et al., 2011; Li et al., 2015; Mints et al., 2010; Mints et al., 2015; Shchipansky et al., 2016). Within the Province, two eclogite associations are distinguished by protoliths: (1) Salma subduction-type association, the protoliths of which are represented by oceanic layered gabbros and basalt flows that contain layers, lenses, and interpillow sediments formed at ~2.9 Ga; (2) Gridino eclogitized mafic dykes. In the Gridino area, in addition to eclogitized dykes, several small eclogite bodies of the subduction type are known, which we consider as a part of the Salma association. Though geochronological data obtained by different authors generally coincide, there are appreciable discrepancies in interpretation of these data. Currently, three different models for the origin and age of metamorphic events in the Belomorian Eclogite Province are proposed. The first one suggests three distinct episodes of eclogite-facies metamorphism: Mesoarchaean and Neoarchaean events related to subduction processes followed by a distinct eclogite-facies event that caused metamorphism of the Palaeoproterozoic Gridino mafic dyke swarm at ~ 2.45–2.40 Ga (Volodichev et al., 2004; Slabunov et al., 2011b; Shchipansky et al., 2012b; Balagansky et al., 2015. The second model assumes a single eclogite-facies metamorphic event at ~1.9 Ga related to the Lapland–Kola Orogeny (Skublov et al., 2010a, 2010b, 2011a, 2011b, 2012; Li et al., 2017a; Liu et al., 2017, Yu et al., 2018). The authors of this paper hold the third model (Dokukina and Konilov, 2011; Dokukina et al., 2010; Dokukina et al., 2012, 2014; Mints et al., 2010, 2014, 2015; Mints and Dokukina, 2020a, 2020b): the Belomorian Eclogite Province was formed during a single tectono-thermal event. Creation of the oceanic crust and eclogite-facies event were constrained to a short time interval between ~2.9 and ~2.78 Ga. A detailed justification for the Archaean age of the eclogite-facies metamorphism, and subsequent metamorphic events, detailed review and criticism of conceptions are given in (Dokukina et al., 2012, 2014; Dokukina and Mints, 2019; Mints et al., 2010, 2015; Mints and Dokukina, 2020a, 2020b).

The main object of our work is kyanite-garnet-phengite-quartz rocks (further Ky-Grt-Ph-Qtz rocks) which were studied in a few eclogite bodies in the Kuru-Vaara quarry. According to numerous attributes, these rocks formed as a result of eclogite-facies metamorphism and subsequent partial melting of alumina-siliceous metasediments localized within the Mesoarchaean oceanic basalt flows (Dokukina et al., 2017). Alumina-siliceous metasediments in the Mesoarchaean komatiite–tholeiite association of the Vedlozero–Segozero greenstone belts can be low metamorphic grade analogues of Ky-Grt-Ph-Qtz rock's protoliths. The aim of this work is U-Pb dating of zircon from the Ky-Grt-Ph-Qtz rocks using LA-ICP-MS and TIMS methods; and $^{40}Ar/^{39}Ar$ dating of white mica.

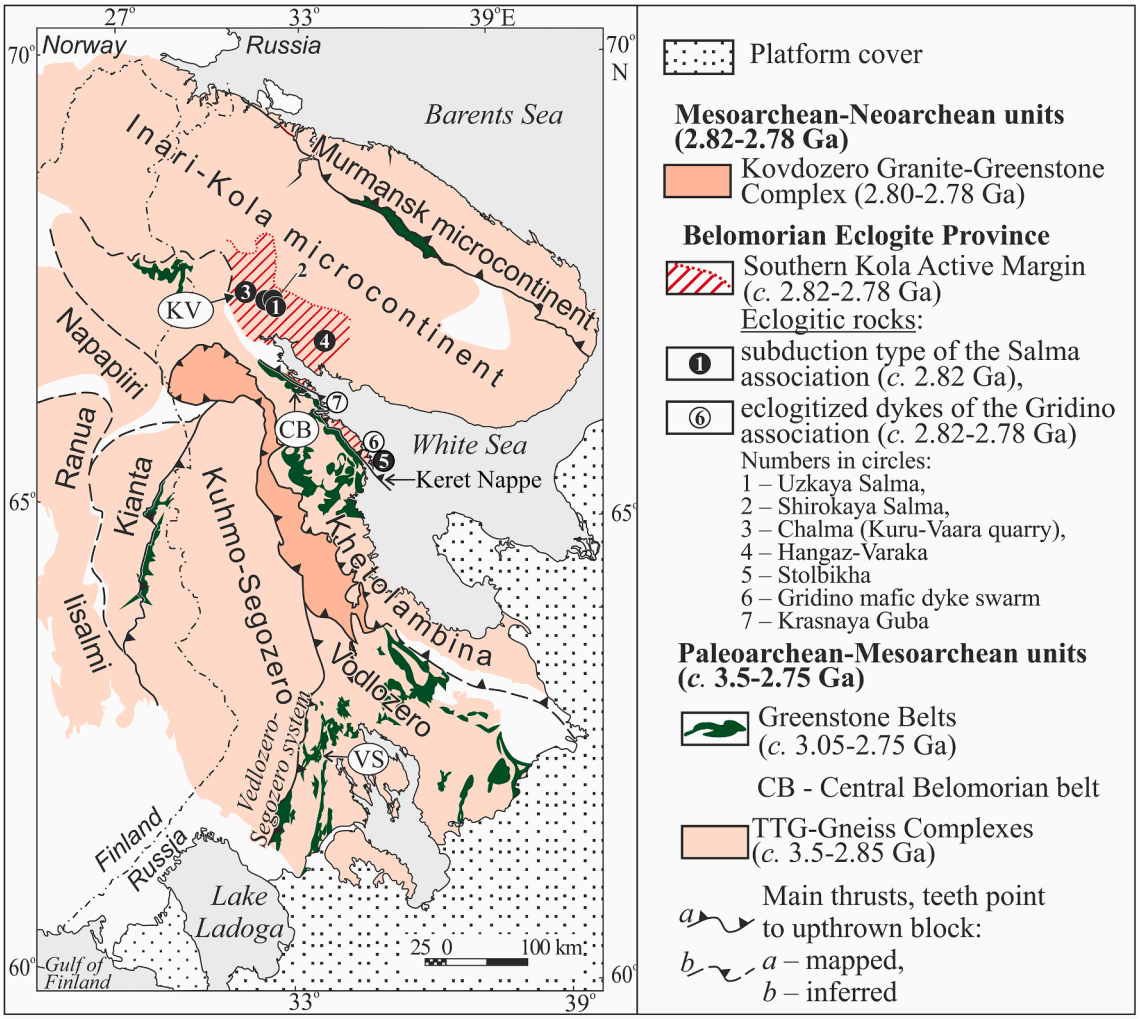

Fig. 1. Tectonic position of the Belomorian Eclogite Province in the northeastern Fennoscandian Shield. Neoarchaean and younger complexes are omitted. The Central Belomorian (CB) and the Vedlozero–Segozero greenstone belts (VS) are mentioned in text; KV is a location of the Kuru-Vaara quarry. Modified after Dokukina et al. (2017).

2. Geological outline.

The lithosphere of the Kola-Karelia region formed during Palaeoarchaean and Mesoarchaean between ~3.5 and ~2.8 Ga as a result of amalgamation of some microcontinents. The most ancient microcontinents (>3.0 Ga) formed due to short-term events of endogenic activity. The formation of younger microcontinents (3.0–2.93 Ga) lasted occasionally down to 2.8 and in some areas down to 2.74 Ga (Fig. 1) (Mints et al., 2015). The microcontinent boundaries are marked by linear greenstone belts up to 200 km long. Rocks of these belts developed into the oceanic, island-arc and back-arc environments and included in the suture zones during microcontinent collisions between 3.05 and 2.85 and 2.88–2.78 Ga and occasionally at 2.84–2.74 Ga (Svetov, 2005; Mints et al., 2010; for more details, see Mints et al., 2015; Mints and Dokukina, 2020a, 2020b).

The Central Belomorian Greenstone Belt ~ 200 km long, that separates the Khetolambina and Inari–Kola microcontinents, is composed of intensely deformed volcanic–sedimentary rocks dated at ~ 2.88–2.85 Ga (Bibikova et al., 1999) (Fig. 1). The available geological, isotopic and geochemical data on mafic–ultramafic rocks of the greenstone complex allow us to interpret them as tectonically disrupted and metamorphosed remnants of the Mesoarchaean ophiolitic association (Slabunov et al., 2006). In contrast to the Central Belomorian Belt, volcanic–sedimentary rocks that make up greenstone belts of the Vedlozero–Segozero system are deformed and metamorphosed not so intensely (Fig. 1). According to Svetov (2005), the volcanic–sedimentary assemblages of the Vedlozero–Segozero greenstone belts are subdivided into two groups: the 3.02–2.91 Ga basalt–andesite–dacite–rhyolite and the komatiite–tholeiite units at the base of the sequence and the ~ 2.90–2.85 Ga andesite–dacite association. The older assemblage is a stratified sequence composed of mafic and ultramafic massive or pillow lavas associated with tuffs, tuffites and sedimentary–exhalative deposit, that is of special interest for our study. Greywacke and conglomerate of the upper sedimentary unit are combined with graphite schist, massive pyrite ore, sedimentary rock and jaspilite. This part of the section also comprises weathered mafic–ultramafic effusive rocks and its weathering products, greywacke with sporadic arkose, and gravelstone lenses. The rocks were metamorphosed into greenschist and epidote–amphibolite facies. The komatiite–tholeiite association is interpreted as a product of back-arc magmatism, presumably with mantle-plume component (Svetov, 2005).

2.1. The Mesoarchaean–Neoarchaean Belomorian Eclogite Province

Subduction of oceanic lithosphere between the Khetolambina and Inari–Kola microcontinents resulted in assembling of these microcontinents and formation of the Belomorian Eclogite Province, which involves marginal parts of both microcontinents and the Central-Belomorian Greenstone Belt (suture zone) plunging to the northeast beneath the Inari–Kola microcontinent. The Khetolambina microcontinent and margin of the Inari-Kola microcontinent formed the collisional overthrust-underthrust ensemble. The structural position of the Inari-Kola margin allows consideration this area as an «active continental margin», despite the absence of reliably identifiable characteristic magmatism. The tonalite–trondhjemite gneiss of the active margin contains large fragments of eclogite sequences and isolated eclogite lenses belonging to the Salma association (Mints et al., 2010, 2014, 2015; Dokukina et al., 2014).

The history of Belomorian eclogites represents following succession of events: (1) forming of the Salma oceanic crust (~2.9 Ga ago) pertaining to the complex of layered gabbro and pillow-basalt, (2) low-grade ocean floor metamorphism, (3) eclogite-facies metamorphism in the course of subduction (minimum pressure of 13.0–14.3 kbar at 770–775 °C) and development of the TTG continental arc along the Southern Kola Active Margin; (4) slab window magmatism (2.87–2.82 Ga) with intrusion of high-temperature (1030–1200 °C) mafic magma into the active continental margin and formation of the Gridino dyke swarm at a hypabyssal crust level (Dokukina et al., 2009, 2010, 2012, 2014; Dokukina and Konilov, 2011; Dokukina and Mints, 2019); (5) subduction and closure of the ocean, collision and amalgamation of microcontinents, and eclogite-facies metamorphism of the subducted crust at 2.82–2.78 Ga (Mints et al., 2014, 2015; Konilov et al., 2011; Shchipansky et al., 2012; Mints and Dokukina, 2020a, 2020b), crustal delamination at the active margin and sinking of the delaminated crust slices together with Gridino mafic dykes, eclogite facies metamorphism of these dykes (Volodichev et al., 2004; Stepanova and Stepanov, 2010; Dokukina et al., 2014; Mints et al., 2015; Dokukina and Mints, 2019).

Further Neoarchaean–Palaeoproterozoic history of the Belomorian Eclogite Province comprises a series of the high temperature (granulite and amphibolite facies) tectono-thermal events related to mantle plumes, accompanied by crystallization and recrystallization of zircon at ~2.74–2.70, 2.5–2.4, and 2.0–1.9 Ga (see in details in Mints et al., 2014, 2015; Mints and Dokukina, 2020a, 2020b) (Fig. 2).

2.2. The Salma eclogite association

The strongly retrogressed eclogites of the Salma association represent large (up to 500 m) eclogite bodies that are tens of kilometres long and small-scale pods and lenses within TTG gneisses (Fig. 3). Gabbronorite is the predominant type of protolith of these eclogites. Eclogites after low-K gabbronorite are closely associated with high-Mg mafic and ultramafic metamorphic rocks (olivine metagabbronorites and metapyroxenites); massive coarse- and medium-grained Fe-Ti eclogites (after Fe-Ti gabbro) with a high content of Fe-Ti oxides; and garnetites. Eclogite facies pillow-basalts are known too. Mafic and ultramafic eclogite-facies rocks can be assigned geochemically to the tholeiite series. Eclogites are strongly amphibolitized: garnet and clinopyroxene are replaced by amphibole. The trace-element abundances point toward a mantle derivation for the magmatic precursors. The inclusions of low- and medium-temperature minerals of the prehnite-pumpellyite and epidote–amphibolite facies similar to derivatives of the hydrothermal metamorphism in the spreading zone and the ocean floor are common in garnet and zircon crystals and some cases in the matrix of the rock (Mints et al., 2010; Konilov et al., 2011). A layering of high-Mg and Fe-Ti eclogitic rocks, their compositional and structural features suggest that the original protolith assemblage resembles the layered gabbroic suite from the modern oceanic crust of slow-spreading ridges, e.g., the Southwest Indian Ridge (Dick et al., 2000).

The most comprehensive and actual review of the geochronological database in rocks of the Salma eclogite association is presented in the recent papers by Mints and Dokukina (2020a, 2020b)). The Fe-Ti eclogites, richest in zircon, contain porous patchy zircon grains with numerous mineral inclusions of quartz, albite, plagioclase, clinopyroxene (diopside), rutile, calcite, muscovite, F-apatite, Al-titanite, pyrite, galena, garnet, amphibole, zoisite/epidote, pumpellyite, chlorite (Kaulina et al., 2010; Li et al., 2017a, 2017b) (Fig. 4a). This zircon contains igneous-type distributions of REE and was recrystallized at coupled dissolution-reprecipitation processes (Mints and Dokukina, 2020a, 2020b). A similar zircon is typical in Fe-Ti ("oxide") gabbro of the modern oceanic crust (Grimes et al., 2008, 2009; Aranovich et al., 2017) and Phanerozoic ophiolites (Kaczmarek et al., 2008). The most reliable age of gabbro crystallization is ~ 2.9 Ga (Mints et al., 2010, 2014, 2015; Mints and Dokukina, 2020a, 2020b). For a long time from ~ 2.9 to ~ 1.9 Ga, the radioactive damage and fluid- or melt-induced alteration of igneous zircon resulted from partially or complete rebalancing of the isotope system.

Round-ovoid zircon grains (Fig. 4b) display obvious attributes of the post-eclogite granulite-facies metamorphism. The round-ovoid zircon displays core-rim structure: structureless or fir-tree in CL cores and light unzoned rims. The cores display HREE enrichment and significant negative Eu anomaly, contain rare single inclusions of garnet, amphibole, plagioclase, quartz, rutile and biotite and yielded ages of 2.73–2.72 Ga. By morphological and geochemical feature, the round-

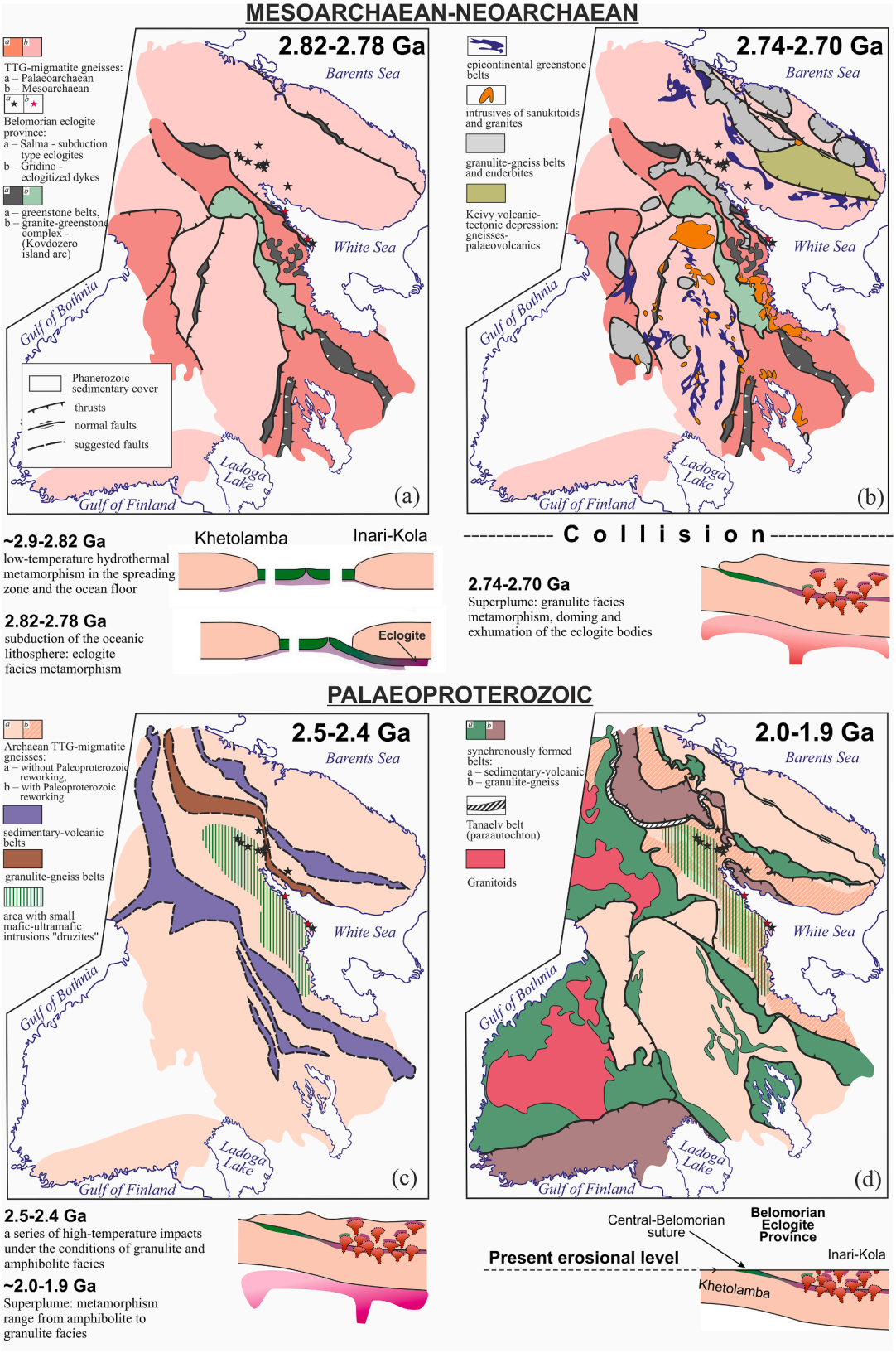

Fig. 2. The Belomorian Eclogite Province within the tectonic structure and Neoarchaean-Palaeoproterozoic history of the Kola-Karelia region. (a) Mesoarchaean-Neoarchaean, 2.90–2.78 Ga, microplate tectonics: formation of the Kola-Karelia palaeocontinent: closure of the oceans separating the microcontinents, subduction of the oceanic lithosphere, the Belomorian Eclogite Province emergence; (b-d) tectonic structures caused by mantle plumes, components of the Global Superplumes: (b) Neoarchaean, 2.74–2.70 Ga: the emergence and evolution of areas of the high-temperature magmatism and metamorphism; (b) Early Palaeoproterozoic, 2.50–2.40 Ga: the initial stage of the combined evolution of granulite-gneiss and low-grade sedimentary-volcanic belts; (c) late Palaeoproterozoic, 2.00–1.90 Ga: the main and final stages of the combined evolution of granulite-gneiss and low-grade sedimentary-volcanic belts.

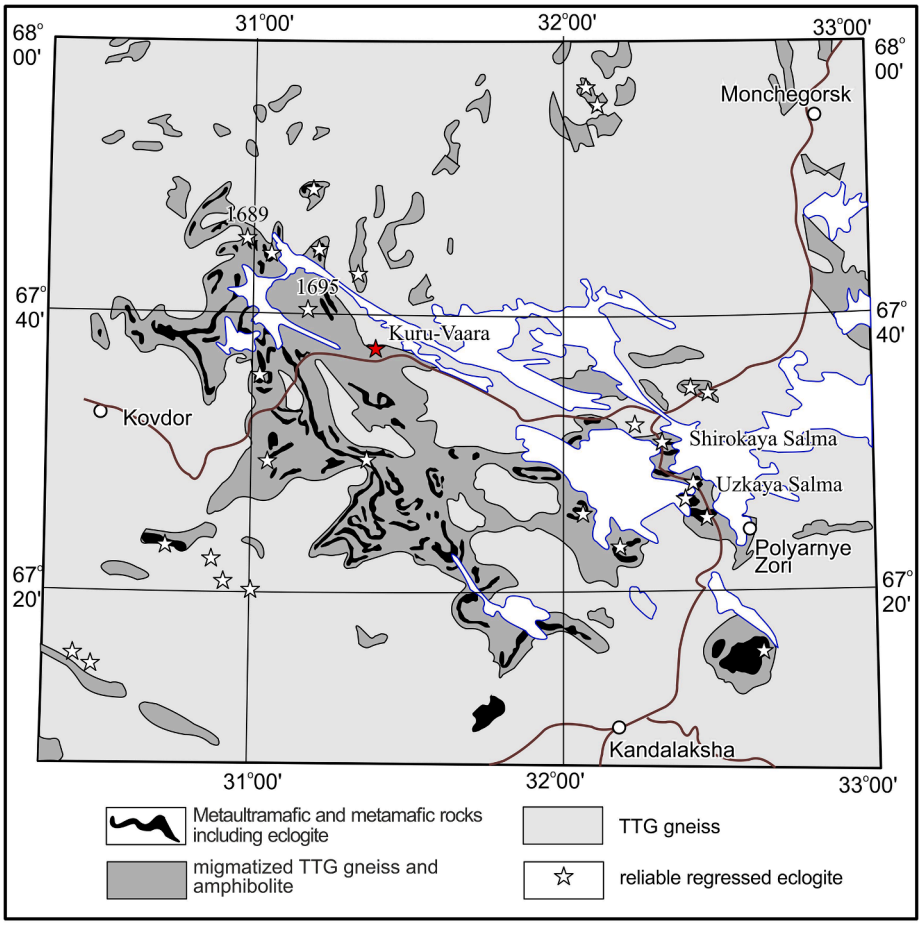

Fig. 3. Geological sketch map of locations, where the known Salma eclogite bodies are shown (after Pozhilenko, 2013).

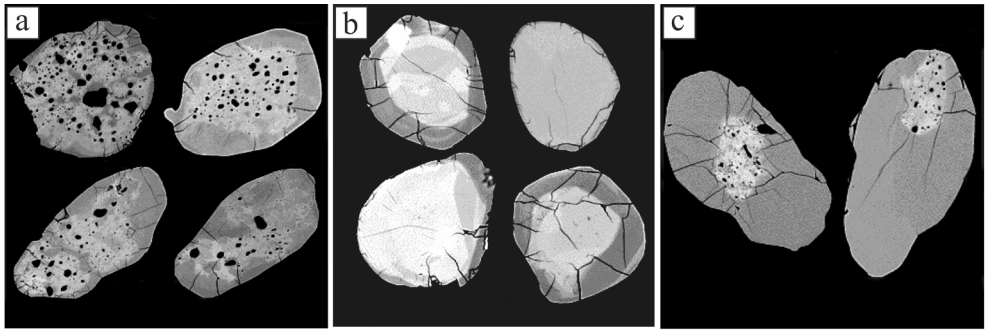

Fig. 4. Specific zircon populations in eclogitic mafic rocks that are related to the successive events in the evolution of the Salma eclogite association (see in detail Mints et al., 2010, 2015; Mints and Dokukina, 2020a, 2020b). The length of the zircon crystals is in the 0.15–0.25 mm range. (a) Fe-Ti gabbro, "porous" zircon with characteristic patchy textures and numerous voids and mineral inclusions (quartz, plagioclase, clinopyroxene, rutile, calcite, muscovite, apatite, Al-titanite, allanite, epidote, pyrite, galena) and high (magmatic-type) concentrations of trace element admixtures including HREE. The most reliable estimate for the crystallization age is ~ 2.9 Ga. A concordant point at 2.82 Ga might represent the age of the earliest metamorphism. (b) The Salma eclogites contain characteristic round-ovoid zircon similar to the "granulite-type" metamorphic zircon. In both cases, the zircon yielded the same age of 2.72–2.70 Ga. (c) The Archaean magmatic and metamorphic zircon cores are often surrounded by low-U unzoned rims with ages of about 1.9 Ga.

ovoid zircon from the Salma eclogites is similar to zircon from the Neoarchaean granulite facies rocks in the Kola-Karelia (Mänttäri and Hölttä, 2002; Kaulina, 2010; Slabunov et al., 2011a) and other regions (Corfu et al., 2003).

Limited zircon grains and late metamorphic zircon rims (Fig. 4c) have Palaeoproterozoic age of 1.88–1.82 Ga (Skublov et al., 2011a; Imayama et al., 2017). The Th/U ratio, generally, is within the 0.01–0.001 range. REE are characterized by low concentrations, flat HREE pattern, and well-pronounced positive Ce and negative Eu anomalies.

3. Methods

3.1. Mineralogy

The chemical analyses of minerals were performed using a Tescan VEGA II XMU scanning electron microscope equipped with both Oxford Instruments WDS Energy 700 and EDS Energy 450 X-ray detection systems at the Institute of Experimental Mineralogy of the Russian Academy of Sciences, Chernogolovka, Moscow Region. Microprobe analysis of coexisting minerals was performed on polished thin sections

after petrographic examination. The operating conditions were: 20 kV accelerating voltage, beam current ~ 350 pA on element (Co) for quant optimization, and a beam diametre of 1–5 μm. When it was necessary to determine the composition of cryptocrystalline mineral intergrowths, the raster mode with beam diametre of 20–30 μm was performed. Acquisition time was 70 s. Dumortierite also examined using EPMA and Raman spectroscopy.

3.2. Geochemistry

Major oxides of whole rock samples were analysed using ARL 9800 X-ray fluorescence (XRF) spectrometer, on samples prepared as $Li_2B_4O_7$ glass discs at the Karpinsky All-Russian Geological Research Institute (VSEGEI), St. Petersburg. International standards are used to calibrate the XRF data. Accuracy and precision are better than ± 2% for the major oxides.

Trace elements were determined using ICP-MS after digestion of the fused pellets with HF + HNO_3. Pure solution external standards were used for calibration and geological (USGS) standards were used to monitor the analytical accuracy. Measurements were performed on an ELAN-DRC-6100l ICP-MS at the VSEGEI. Precision for REEs was better than 5%, whereas the precision for Rb, Sr, Ba, Nb, Ta, Zr, Hf, U and Th was better than 10%.

3.3. Geochronology

Mineral monofractions were separated using heavy liquids, magnetic separator and hand picking at the Geological Institute of the Russian Academy of Sciences (Moscow).

Conventional U–Pb dating of zircon, samples 4LMy4-12, 4LM901 and 4LM904 was conducted at the Geological Institute of the Kola Science Centre. Chemical digestion of the minerals and U and Pb extraction were done using the method by Krogh (1973). Uranium and lead contents were determined by isotopic dilution with a $^{208}Pb/^{235}U$ tracer on MI-1201T and Finnigan MAT 262 mass spectrometers. The site coordinates and isotope ages were calculated using the Isoplot 4.15 software (Ludwig, 1999, 2000).

The U-Pb zircon of samples 4LMy4-12-5 and 4LMy2-3 dating was performed using LA–SF-ICP-MS method in the "Analytical Centre of Mineralogical, Geochemical and Isotope Studies" at the Geological Institute, SB RAS Ulan-Ude, Russia. The method is described in Supplementary methods.

U-Th-Pb zircon dating of sample 4LMy2-9, 4LM901 and 4LM904 was performed using LA-ICP-MS method in the Geological Institute of Russian Academy of Sciences (GIN RAS), Moscow, employing a sector field - inductively coupled plasma – mass spectrometer (SF-ICP-MS) Thermo Scientific Element 2 coupled to Electro Scientific NWR-213 laser ablation system (see Supplementary method).

$^{40}Ar/^{39}Ar$ dating of white mica (sample 4LMy2-3). For the $^{40}Ar/^{39}Ar$ dating, samples of mica mineral fractions, together with those of MSA-11 biotite (OSO no. 129-88), were packed in Al foil and sealed in an evacuated quartz capsule. Biotite sample MSA-11, prepared at the Fedorovsky All-Russian Scientific Research Institute of Mineral Resources in 1988 as a standard for K–Ar dating, was certified as an $^{40}Ar/^{39}Ar$ monitor with the help of international standard samples: Bern 4 m muscovite and LP-6 biotite (Baksi et al., 1996). The average calibrated value (311.0 ± 1.5 Ma) was taken to be the integrated age of MSA-11 biotite. Afterward, the grains were irradiated in a Cd-plated channel of a VVR-K scientific reactor (Institute of Nuclear Physics of Tomsk Polytechnic University, Tomsk). The neutron-flux gradient did not exceed 0.5% of the sample size. Experiments on incremental heating were performed in a quartz reactor with an external furnace. Blank experiment for ^{40}Ar (10 min at 1200 °C) did not exceed 5 × 10–10 ncm^3. Argon was purified with Ti and ZrAl SAES getters. The Ar isotope composition was determined on Noble Gas 5400 (Micromass, United Kingdom) and multi-collector mass spectrometer ARGUS. 1200 °C blank of ^{40}Ar deed not exceed $n*10^{-9}$ STP. The measurement error in the text, tables, and figures is within ± 1σ.

3.4. Zircon composition

Trace elements concentrations in zircon grains were determined using the high-resolution mass spectrometer Element 2 (Thermo Fisher Scientific, Germany) and laser ablation system NWR-213 Nd-YAG, (ESI, USA) in the Geological Institute of Russian Academy of Sciences (GIN RAS), Moscow. Ablation was carried out at spot size of 40 μm, 5 Hz, and actual fluence of 5–6 J/cm^2 at the sample surface. Helium was used as a transport aerosol gas. Isotopes ^{49}Ti, ^{88}Sr, ^{89}Y, ^{91}Zr, ^{93}Nb, ^{139}La, ^{140}Ce, ^{141}Pr, ^{146}Nd, ^{147}Sm, ^{151}Eu, ^{157}Gd, ^{159}Tb, ^{163}Dy, ^{165}Ho, ^{167}Er, ^{169}Tm, ^{173}Yb, ^{175}Lu, ^{177}Hf, ^{181}Ta, ^{208}Pb, ^{232}Th and ^{238}U were measured.

Trace elements concentrations were calculated using zircon 91500 as a primary reference material and Zr for internal standardization. Zircon crystals Plešovice and GJ-1 were measured for quality control. Data reduction was performed offline with Glitter software.

3.5. Fluid inclusions study

Fluid inclusions were studied in double-polished plates (200–300 μm thick) using a Linkam heating/freezing stage with a working temperature of −196 °C to 600 °C (THMSG 600) and an automated sample heating–cooling with rates from 0.1 °C to 90 °C/min reproducible to 0.1 °C. The stage was systematically calibrated using natural carbon dioxide (Camperio, Alps) and synthetic aqueous inclusions in quartz. Changes in the inclusions were observed under an optical microscope or with a digital video camera. The composition of fluid inclusions was analysed on a RM1000 (Renishaw) single-channel Raman spectrometer with Ar laser.

3.6. X-ray diffraction

Semiquantitative mineralogical composition of clay minerals were analysed in laboratory of XRD methods of the Department of Oil-Gas Sedimentology of M.V. Lomonosov Moscow State University with a Rigaku MiniFlex II X-ray diffractometer. The primary analytical data were processed through PDX2. The clay fraction (<2 μm) was obtained by the sedimentation method as described (Moore and Reynolds, 1997; Hillier et al., 2003).

4. Rock descriptions

Borosilicate-, garnet–, phengite-, kyanite- and corundum-bearing quartz rocks are found within the retrogressed eclogite blocks in the Kuru-Vaara quarry (Fig. 5). Tabular or lenticular leucocratic Ky-Grt-Ph-Qtz bodies are a few centimetres to several decimetres thick and are characterized by rectilinear or smoothly curved contacts and formed a network, which divides eclogites into rounded or angular blocks a few decimetres in size (Fig. 5a, b). The relatively thick tabular bodies represent leucocratic interlayers that are heterogeneous in composition (Fig. 5c). Some bodies are fully modified under later granulite-facies metamorphism (Fig. 5d).

The relationship of eclogites in Kuru-Vaara with non-linear thin Ky-Grt-Ph-Qtz streaks almost exactly mimics the structure of pillow lavas with interpillow fill composed of hyaloclastites and alumina-siliceous sediments in the Mesoarchaean Vedlozero–Segozero greenstone belts (Dokukina et al., 2017) (Fig. 5h).

4.1. Petrography

Mineral abbreviations used in figures and reactions are after Whitney and Evans (2010).

Eclogite. The petrography of the Salma eclogites was described in detail earlier (Konilov et al., 2011; Shchipansky et al., 2012a, 2012b;

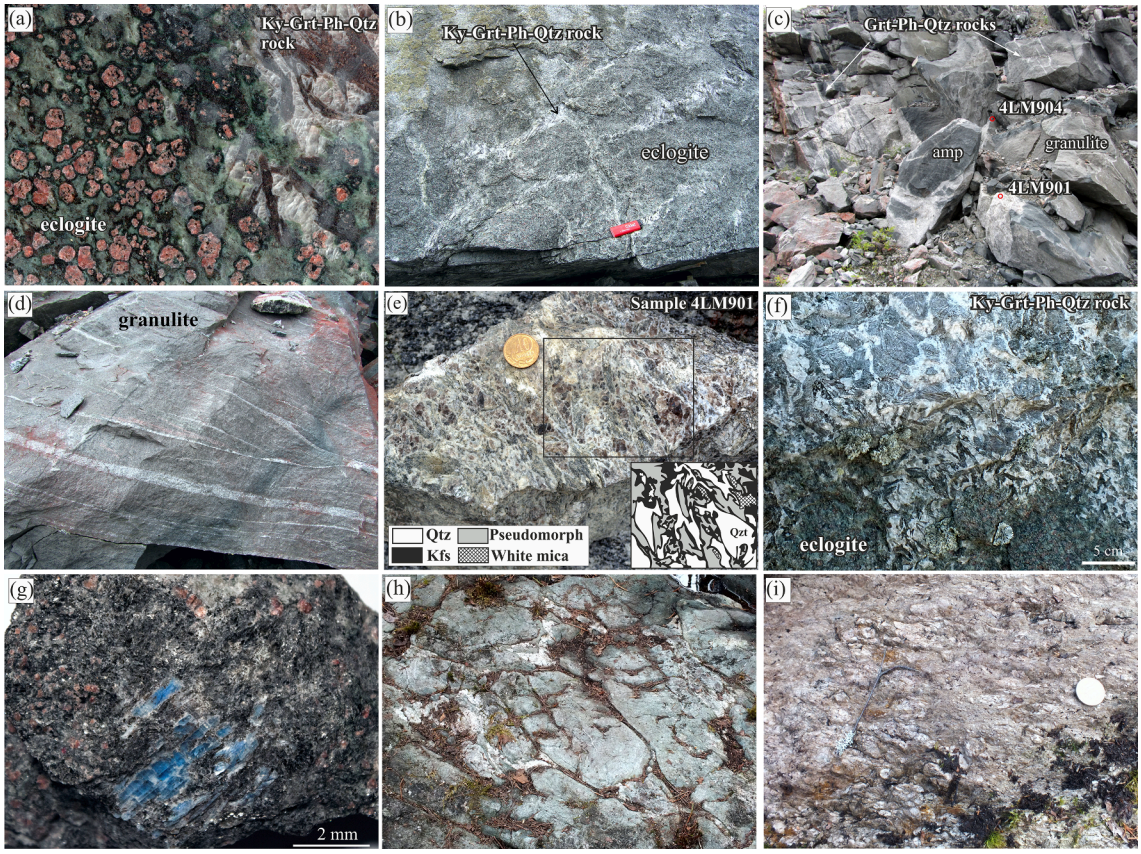

Fig. 5. Photos of outcrops and samples of the Kuru-Vaara quarry metamorphic rocks (a-g) and the Mezoarchaean volcano-sedimentary rocks of the Vedlozero–Segozero greenstone belts (h, i): (a) Polished surface of a rock sample where the ratio between the retrogressed symplectite eclogite and the Ky-Grt-Ph-Qtz rock is shown; (b) an outcrop of the eclogite – the Ky-Grt-Ph-Qtz rock association retaining relic features of pillow lava with interpillow fill; (c) tabular bodies of Ky-Grt-Ph-Qtz rocks hosted in leucocratic interlayer heterogeneous in composition and parallel thin veins hosted in eclogite; (d) tabular bodies of Ky-Grt-Ph-Qtz rocks hosted in post-eclogitic granulite; (e) a hand sample of Ky-Grt-Ph-Qtz rock; (f) a surface of Ky-Grt-Ph-Qtz rock in symplectite eclogite; (g) a hand sample of coarse kyanite grains grown at boundary between the symplectite eclogite and the Ky-Grt-Ph-Qtz rock. (h) Pillow-basalt lava with the interpillow space filled the sedimentary material, the Koikar structure of the Vedlozero–Segozero greenstone belts; (i) the alumina-siliceous sedimentary rocks from the upper part of the volcano-sedimentary sequence, the Koikar structure.

Balagansky et al., 2015; Liu et al., 2017; Li et al., 2017a, 2017b; Yu et al., 2018). A typical retrogressed eclogite consists of poikilitic garnet porphyroblasts (3–5 mm, on average) in a fine-grained light-green groundmass of Na-poor clinopyroxene + plagioclase symplectite after omphacite, and minor amphibole and quartz (Figs. 5a, 6a). Garnet contains pre-eclogite low-temperature and low-pressure mineral inclusions (albite, chlorite, pumpellyite, actinolite, etc.); quartz, rutile; and is rimmed by hornblende, plagioclase, and quartz kelyphitic rims (Fig. 6a). Omphacite relicts free of inclusions or with oriented quartz needles are found locally in the symplectite, yet most samples show a complete breakdown of omphacite to clinopyroxene-plagioclase symplectite. Orthopyroxene occasionally is found in the clinopyroxene–plagioclase symplectite as evidence for decompression metamorphic trend in the *PT*-space of granulite facies (Page et al., 2003; Groppo et al., 2007; Konilov et al, 2011). At some sites, the symplectite eclogites was replaced by garnet-clinopyroxene-plagioclase granulite-facies assemblage (Fig. 6b, c).

At the contact with Ky-Grt-Ph-Qtz rocks, mafic rocks are represented by varieties of symplectite eclogite (Fig. 5a) or are completely replaced with garnet–clinopyroxene–plagioclase granulite (Figs. 5d, 6b-f). In some cases, a transitional zone is found at the contact, where mineral assemblages are garnet, clinopyroxene–plagioclase symplectite with K-feldspar, biotite, and augen quartz segregations.

Kyanite-garnet-phengite-quartz rock. This rock is characterized by an augen-like structure expressed in large (up to 5 cm) angular mono- or polycrystalline quartz aggregates (20–60% of rock volume); monocrystals and glomerocrysts of euhedral phengite in quartz, kyanite or/and polymineralic aggregates (50–35 vol%), which are separated from quartz by feldspar moats (10–25 vol%) (Figs. 5a, e-g; 7).

Scarce single euhedral phengite flakes or phengite glomerocrysts (Fig. 7d) in quartz are up to 10 mm long and more. Euhedral coarse grains of primary kyanite up to 10 mm contain garnet inclusions (Fig. 7i) and occasionally replaces by high-temperature plagioclase ± sapphirine ± spinel intergrowths at a reaction of kyanite with garnet. Sapphirine and spinel have vermicular shape and form symplectite rims around kyanite. Followed retrograde muscovite + feldspar irregular intergrowth formed after plagioclase (Fig. 7i).

The observed transformation sequence of phengite mica into polymineralic pseudomorphs was established (Fig. 7d-f). The phengite was replaced by moats of feldspar, biotite and kyanite. Relicts of phengite monocrystals or phengite intergrowths are rarely retained in polymineralic pseudomorphs; however, most commonly phengite completely disappears and is replaced by a polymineralic aggregate, which is separated from quartz by a feldspar moat.

In the most abundant pseudomorphs, the cores composed of biotite + plagioclase ± kyanite and garnet symplectites are rimmed by zonal feldspar moats (Fig. 7). The complex pseudomorphs are consisted of muscovite and/or biotite, kyanite, K-feldspar, plagioclase, zircon and rutile occasionally with less frequent garnet, dumortierite, and corundum (Fig. 7c, d). The space between albite and the pseudomorph core occasionally is filled with mesoperthite, i.e., regular K-feldspar segregations in the plagioclase matrix (Fig. 7g). In the pseudomorphs,

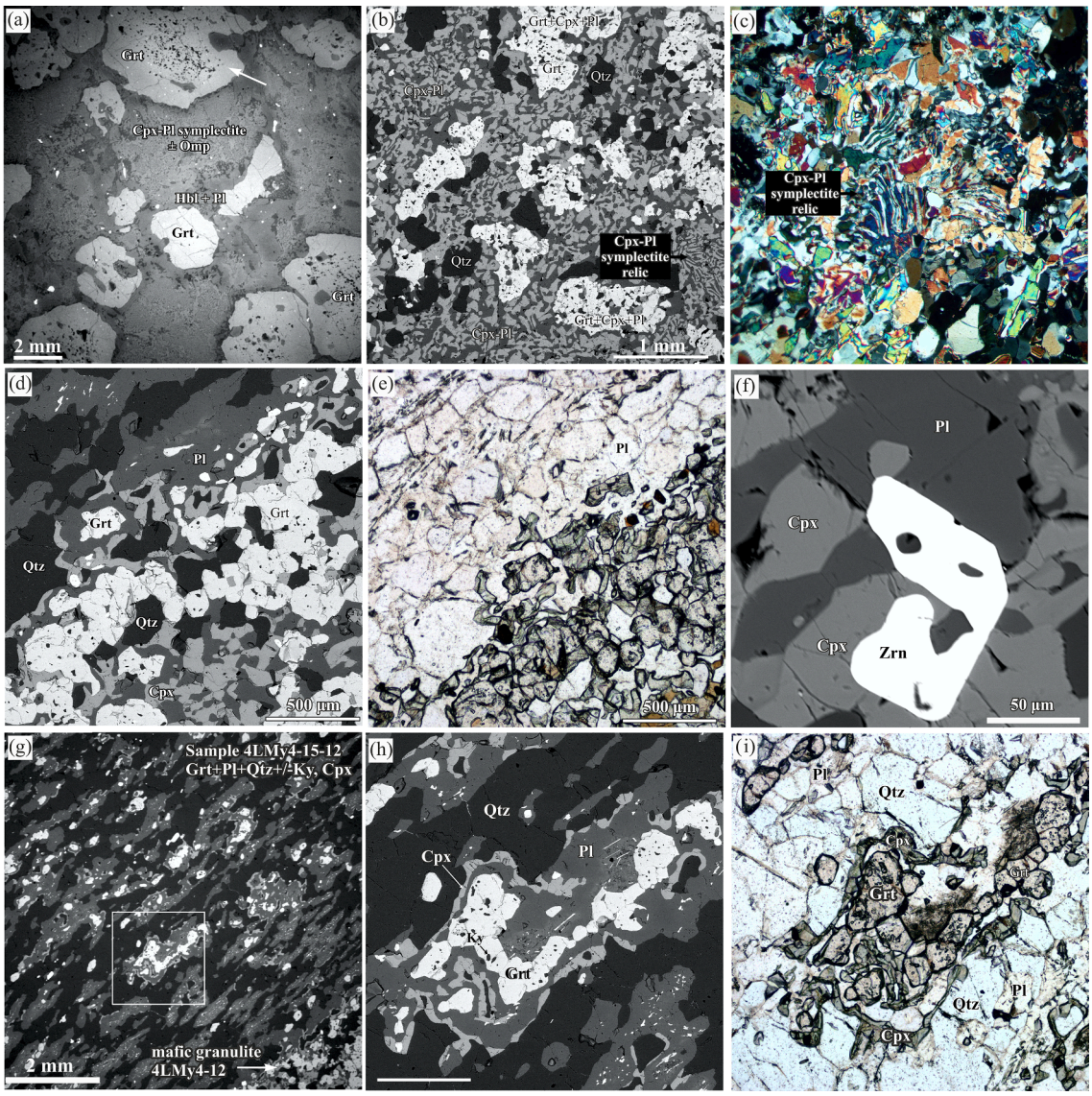

Fig. 6. Back-scattered electron (BSE) images and photomicrographs of mafic and felsic rocks: (a) BSE image of symplectic eclogite, sample 4LMy4-15–1. The arrow shows a garnet in Fig. 8a; (b-f) Sample 4LMy4-12: BSE image (b) and cross polarized light (XPL) photomicrograph (c) of relicts of Cpx-Pl symplectite retain among granoblastic garnet–clinopyroxene–plagioclase aggregate that represents recrystallized eclogite; BSE image (d) and plan polarized light (PPL) photomicrograph (e) of recrystallized eclogite as granoblastic garnet–clinopyroxene–plagioclase granulite aggregate at contact with Ky-Grt-Ph-Qtz thin vein-like rock (sample 4LMy4-12–5); (f) BSE image of zircon within Grt-Cpx-Pl granulite aggregate ; (g-i); Sample 4LMy2-15–5: BSE image (g) of residual variety of Ky-Grt-Ph-Qtz rocks with garnet, plagioclase, quartz and clinopyroxene; BSE image (h) and PPL photomicrograph (i) of the enlarged fragment in a white square from (g). Mineral abbreviations after (Whitney and Evans, 2010).

that consist of biotite + kyanite + K-feldspar, the K-feldspar contains submicroscopic albite lamellae.

Dumortierite in the studied samples reveals pleochroism in red hues. Corundum and kyanite are found in pseudomorphs close to each other but do not come into mutual contacts. An appearance of silica-deficient corundum in rocks with abundant free quartz is an unusual phenomenon mostly related to ultrahigh-temperature metamorphism (Kelsey, 2008). Corundum is found only within pseudomorphs and never in contacts with quartz. Platelets and needles of kyanite, corundum and dumortierite occupy cleavage planes in mica.

In some cases, Ky-Grt-Ph-Qtz rocks have areas with mineral associations different from those described above. Quartz contains calcite and allanite segregations and veinlets. The round fragments, veinlets and large areas consist of epidote-group minerals (zoisite, allanite, epidote) (Fig. 7h), Ca-plagioclase, clinopyroxene, grossular, amphibole, and quartz, nodules and vein-like bodies a few centimetres across consist of garnet–quartz-plagioclase (±clinopyroxene) intergrowths (Fig. 6e, f; 7i).

4.2. Mineral compositions

Petrology and mineralogy of the Ky-Grt-Ph-Qtz rocks are described in detail earlier (Dokukina et al., 2017). Representative mineral compositions for eclogite, granulite and Ky-Grt-Ph-Qtz rock are summarized in Table S1.

Eclogite. Garnet in the symplectic eclogite is characterized by prograde zoning with increase of pyrope content from core ($Alm_{38-42}Prp_{32-36}Grs_{22-24}Sps_{1-2}$) to rim ($Alm_{35-36}Prp_{40-44}Grs_{19-22}Sps_{1}$) (Fig. 8a). Recrystallized garnet in granulitized eclogites has heterogeneous compositions, some of which are relicts of the primary eclogite composition (Fig. 8b). The jadeite content in omphacite relicts is up to 29–31 mol %. Symplectic clinopyroxene intergrown with sodic plagioclase (oligoclase and andesine, An_{20-40}) contains Na per formula unit of 0.05–0.11. Relicts of bytownite (An_{84-85}) are found locally in symplectite domains.

Kyanite-garnet-phengite-quartz rock. The euhedral phengite is characterized by high Si (3.27 to 3.33 Si cations per 11 oxygen atoms) and

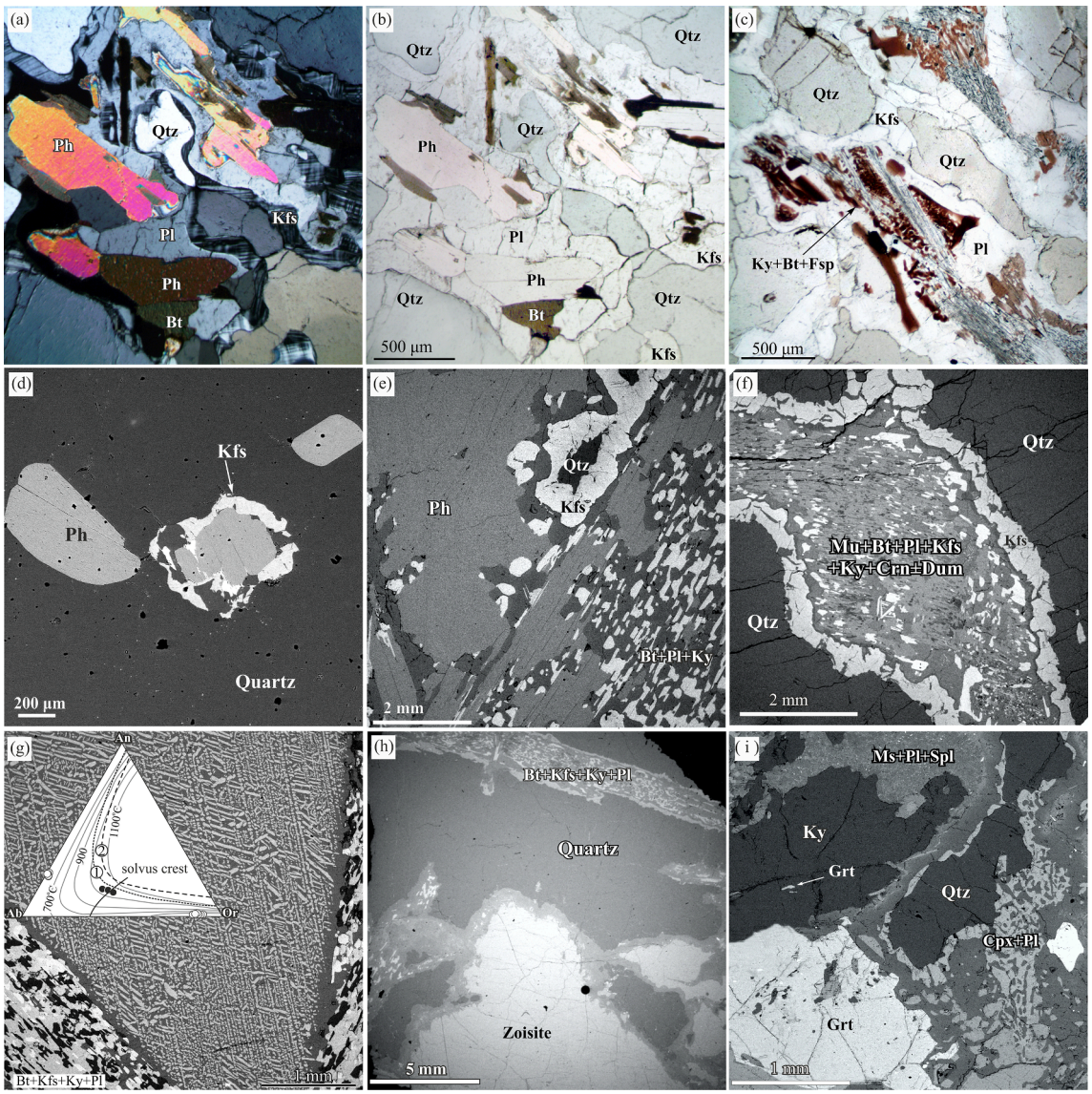

Fig. 7. BSE images, XPL and PPL photomicrographs of Ky-Grt-Ph-Qtz rocks. (a-c) Phengite breakdown with forming of polymineralic pseudomorphs consisting of biotite, plagioclase, K-feldspar, and kyanite in quartz. (d-f) BSE images to show the successive stages in the formation of pseudomorphs after phengite: (d) unreacted phengite and onset of melting with the formation of feldspathic moat, sample 4LMy2-6; (e) pseudomorphs with phengite relicts in the core (sample 4LMy2-10); (f) complete pseudomorph after phengite (sample 4LMy1-5b). (g) BSE image showing mesoperthite replacing feldspar, sample 4LMy4-15–7). Reintegrated compositions of subsolidus feldspar; the solvus curve at 8 kbar is after Hokada (2001). White circles are feldspar compositions in the mesoperthite, whereas black circles are the reintegrated compositions of primary feldspar. Numbered curves for 1100 °C are after Lindsley and Nekvasil (1989), curve (1), and Elkins and Grove (1990), curve (2); (h-i) Compositional heterogeneity of Ky-Grt-Ph-Qtz rocks: BSE images of (h) zoisite inclusion within Ky-Grt-Ph-Qtz rock (samples 4LMy4-15-4b); (i) resorbed garnet and clinopyroxene-plagioclase-quartz symplectite within Ky-Grt-Ph-Qtz rocks localized in retrogressed eclogite (sample 4LMy4-15-3b).

elevated MgO (2.16–2.66 wt%).

The most magnesian garnet ($Alm_{31}Prp_{48}Grs_{20}Sps_{1}$) is found within coarse kyanite blades (Fig. 7i). In some cases, garnet in the pseudomorphs records pronounced retrograde zoning with high pyrope content in the core ($Alm_{35\text{-}54}Prp_{24\text{-}40}Grs_{20\text{-}24}Sps_{1\text{-}2}$) and low pyrope content at the margins ($Alm_{55\text{-}61}Prp_{14\text{-}23}Grs_{11\text{-}20}Sps_{3\text{-}10}$) (Fig. 8b). In other cases, garnet in the pseudomorphs is found as sporadic grains characterized by relatively constant composition ($Alm_{51\text{-}57}Prp_{16\text{-}21}Grs_{18\text{-}23}Sps_{2\text{-}4}$) (see for example Fig. 6g-i).

Feldspars in complex pseudomorphs are characterized by variable compositions. In some cases, the feldspar coronas are zoned. K-feldspar at the quartz boundary replaces albite (An_3), which replaces oligoclase toward the core of the pseudomorph, where both K-feldspar and plagioclase or only a single feldspar may occur. Reintegrated composition of subsolidus feldspar that was formed before mesoperthite is $An_{14\text{-}16}Ab_{45\text{-}52}Or_{32\text{-}39}$ (Fig. 7g). Kyanite replaces by Ca-plagioclases (labradorite – anorthite).

Dumortierite contains of significant MgO (1.29 ± 0.14 wt%) and TiO_2 (2.46 ± 0.25 wt%); Nb-bearing rutile (Nb_2O_5 up to 4–5 wt%) and Th-rich zircon are widespread in Ky-Grt-Ph-Qtz rock (Fig. 9); for details, see "Geochronology" section.

4.3. Fluid inclusions in quartz

CO_2-rich and aqueous-salt fluid inclusions trapped in large relic quartz grains were investigated in Ky-Grt-Ph-Qtz rocks (Fig. 10a-c). We studied fluid inclusions in quartz monocrystals, that contain unaltered phengite (Fig. 8d). The CO_2-rich inclusions are light, relatively small (no larger than 5–10 μm), round, with sharp boundaries. Larger (15–20 μm) inclusions of irregular or negative crystal shapes are less common.

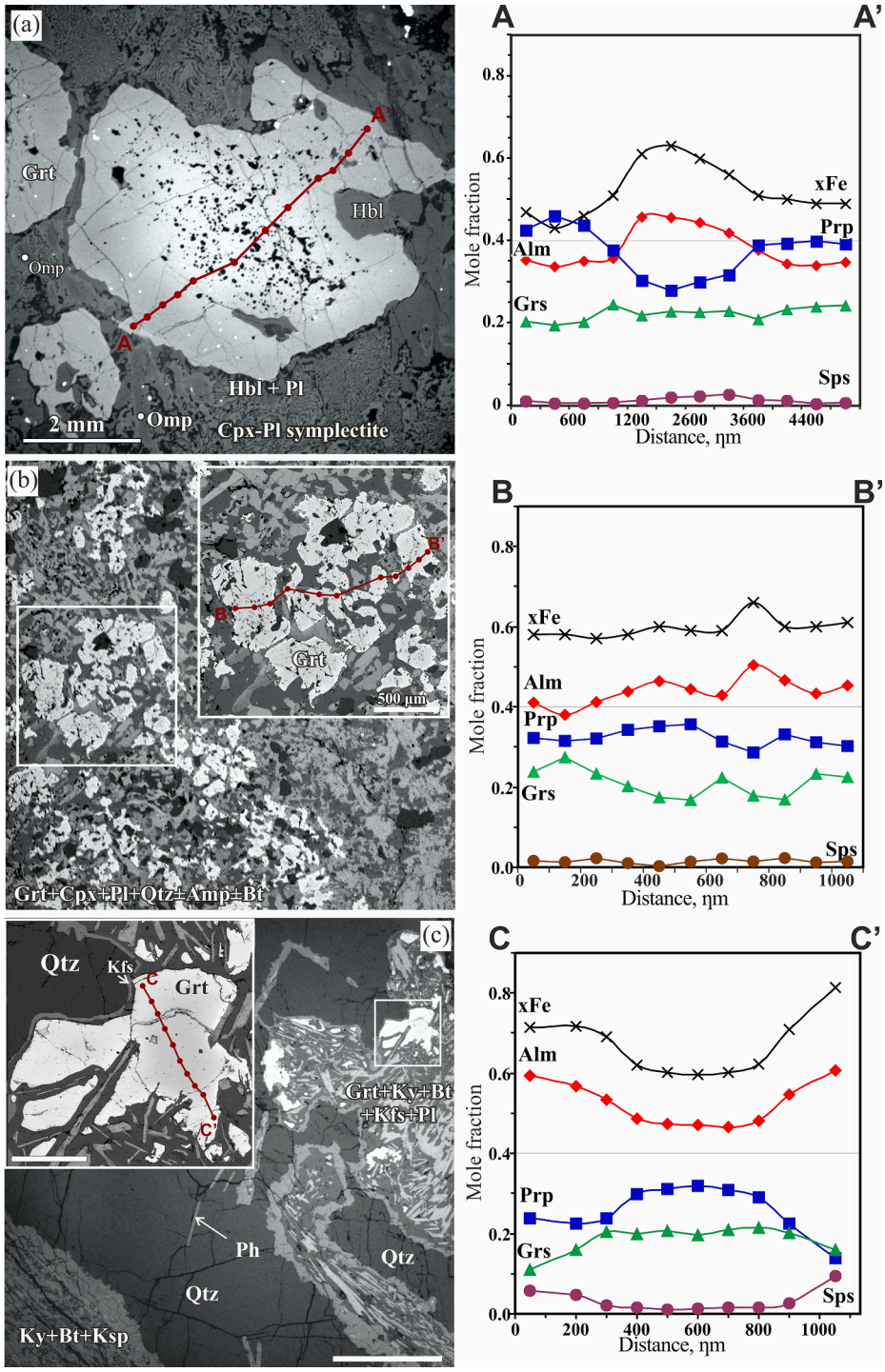

Fig. 8. (a) BSE image of eclogite garnet marked by an arrow in Fig. 6a, sample 4LMy2-15–1. A–A' line is the compositional profile of garnet; (b) BSE image granoblastic garnet–clinopyroxene–plagioclase aggregate representing recrystallized eclogite; garnet close-up fragment, sample 4LMy4-12. B–B' line is the compositional profile of garnet; (c) BSE image of unaltered phengite monocrystals within quartz and phengite breakdown to various degree and pseudomorphs after phengite consisting of biotite, plagioclase, K-feldspar, and kyanite with garnet in quartz; garnet close-up fragment, sample kv06-19an. C–C' line is compositional profile of garnet.

Primary inclusions are concentrated in a form of isolated groups (Fig. 10a), pseudosecondary inclusions are spatially restricted to healed cracks (Fig. 10b). Two main generations of CO_2-rich inclusions are recognized. The identification of generations is based on their textural differences (primary, pseudosecondary, and secondary inclusions); mutual relationships, e.g., crosscutting relations between healed fractures; variation in homogenization temperature and density; and Raman spectroscopy (Fig. 10d). The first generation comprises high-density primary inclusions (ρ = 1.108–1.056 g/cm^3) with a low homogenization temperature down to −37.9 °C. The melting temperature of these inclusions varies within a range of −57.8 to −58.3 °C (Fig. 10e). Some depression of T_m in comparison with −56.6 °C for pure carbon dioxide is caused by an admixture of additional components, probably 1–3 mol % nitrogen. The second generation of CO_2-rich pseudosecondary inclusions is characterized by homogenization temperatures that range between −33.6 and −6.8 °C (ρ = 1.091–0.966 g/cm^3) and melting temperature from −57.4 to −58 °C.

Salt-bearing aqueous pseudosecondary inclusions are localized in healed fractures (Fig. 10c). The inclusions are light-pervious, isometric in shape, with drawn-out ends and no larger than 10–25 μm in size. The sample contains numerous smaller inclusions 5–10 μm in size. The initial ice melting temperature varies from −58 to −51 °C and suggests a probable presence of $CaCl_2$, NaCl and $MgCl_2$ in the fluid (Fig. 10e). The final melting temperature varies from −14.3 to −7.7 °C and corresponds

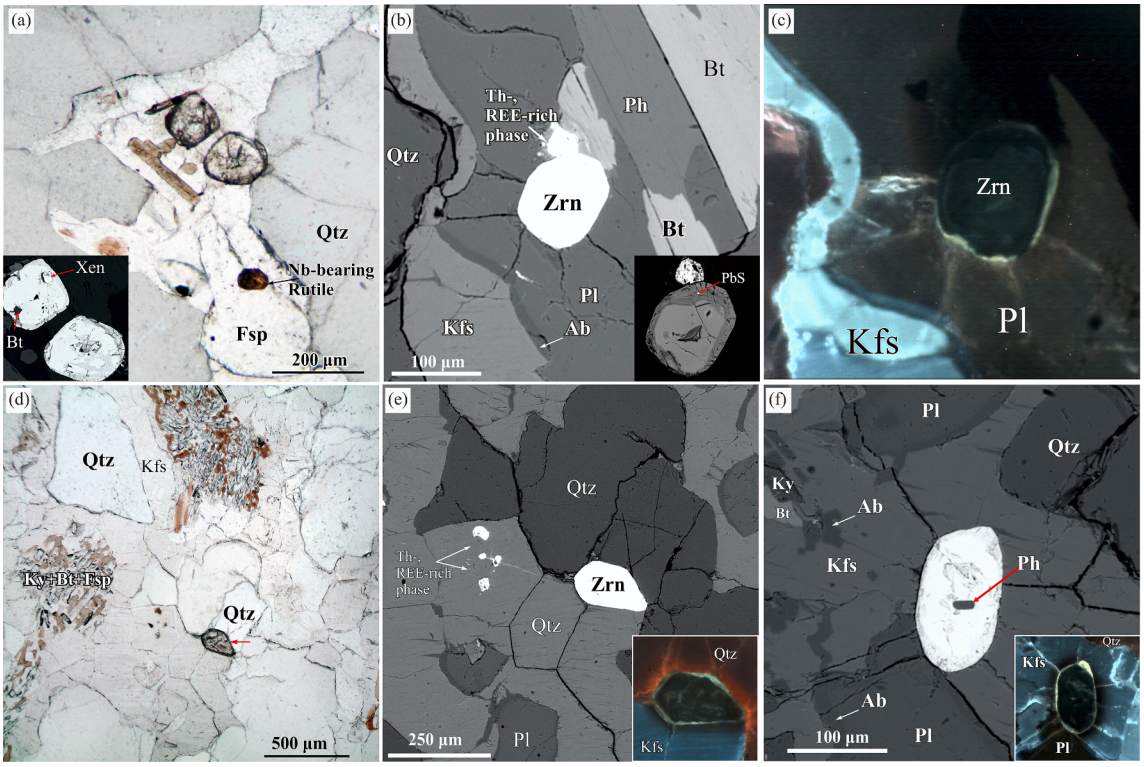

Fig. 9. Zircon within polymineral pseudomorphs, sample 4LMy2-9: (a) PPL photomicrograph and BSE image; (b) BSE image; (c) cathodoluminescence (CL) images of zircon from (b); (d) PPL; (e) BSE and CL images of zircon from (d); (f) BSE and CL images.

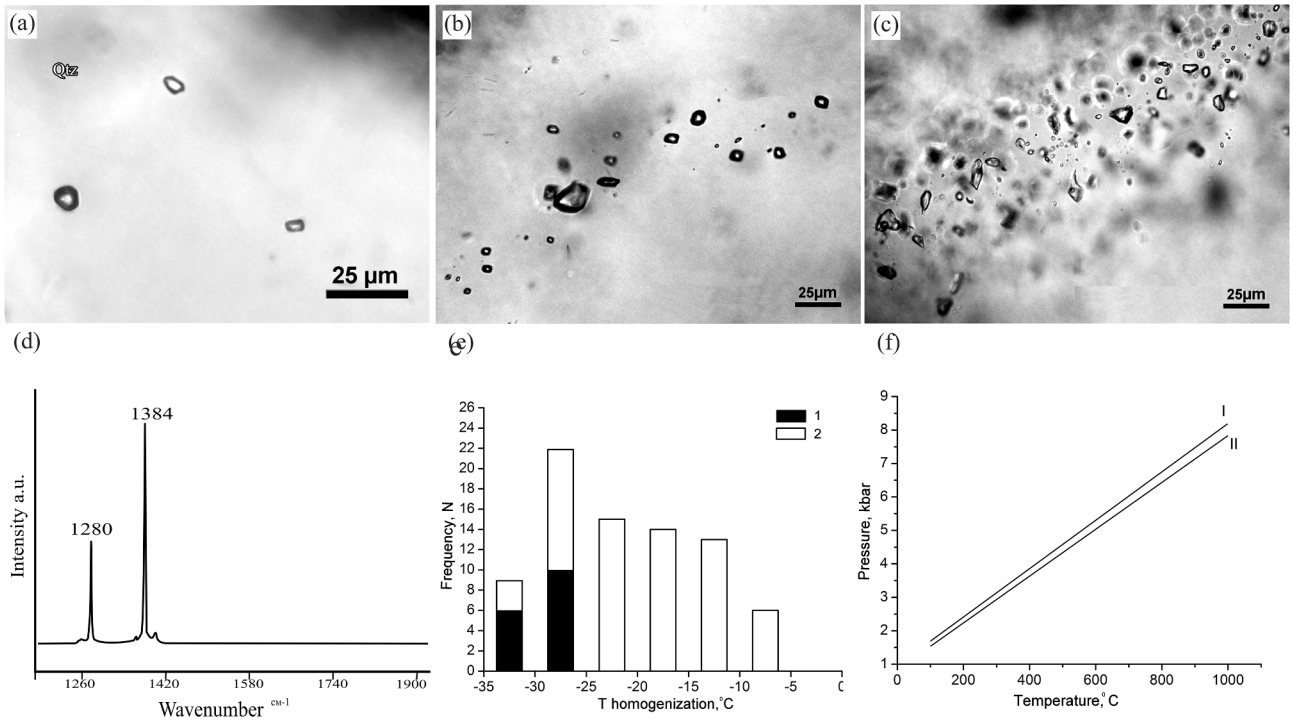

Fig. 10. (a-c) Photomicrographs of fluid inclusions in quartz: (a) CO_2 primary inclusions; (b) CO_2 pseudosecondary inclusions; (c) Salt-bearing aqueous pseudo-secondary inclusions. (d) Raman spectra of CO_2 fluid inclusions; (e) histogram of homogenization temperatures of CO_2 inclusions: 1 - primary inclusions, 2 - primary-secondary inclusions; (f) calculated isochores of CO_2 fluid inclusions: I - primary inclusions, II - primary-secondary inclusions.

to 18.18–11.35 wt% NaCl eq. The pseudosecondary salt-bearing aqueous inclusions are frequently associated with pseudosecondary CO_2-rich inclusions that provide evidence of synchronous entrapment.

4.4. Geochemistry

Eclogites. Salma eclogites correspond mainly to oceanic type low-K

tholeiite in bulk chemical composition (Mints et al., 2010, 2014; Konilov et al., 2011; Shchipansky et al., 2012b). The eclogites that host Ky-Grt-Ph-Qtz rocks somewhat are specific in composition. They are characterized by elevated SiO_2 (51–54 wt%), low FeO (7.7–9.0 wt%), and MgO (7.8–8.5 wt%) concentrations relative to N-MORB-type eclogites: SiO_2 45–50, FeO 9.2–11.6, and MgO 7.8–12.3 wt% (Fig. 11, Table S2). The eclogites that contain the Ky-Grt-Ph-Qtz rocks are enriched in LREE (La_N/Lu_N = 2.9–4.3), vary in Zr and Hf contents, have negative Ta and Nb anomalies and Nb_N/Th_N = 0.2–0.6 in contrast to N-MORB-type rocks with La_N/Lu_N = 0.40–0.86, Nb_N/Th_N = 1.0–2.3 (Fig. 12a, Table S2). Both types of eclogite lack Eu anomalies (Fig. 12b).

Kyanite-garnet-phengite-quartz rock. Samples of this rock were taken from the outcrop, where a relatively large body of compositionally heterogeneous Ky-Grt-Ph-Qtz rocks, as well as a series of thin parallel vein-like bodies hosted in eclogite are overprinted by granulite facies mineral assemblages. These rocks display high SiO_2 content (70.0–79.9 wt%) and magnesium number (X_{Mg} 0.57–0.78) along with low magnesium and iron contents (MgO = 0.49–1.65 wt%, FeO = 0.66–1.90 wt%). The Al_2O_3 content varies from 11.5 to 17.0 wt%; A/CKN = Al_2O_3/(CaO + K_2O + Na_2O) ratio (molecular quantities) is 1.05–1.57. Except for sample 4LMy4-12, the rocks are characterized by elevated contents of alkalies (1.7–4.8 wt% K_2O, 2.1–2.6 wt% Na_2O) and low concentrations of other major elements (Fig. 11, Table S2). The Ky-Grt-Ph-Qtz rocks are enriched in LREE (La_N/Lu_N = 20, Lu_N/Sm_N = 0.16–0.24) and display negative Eu anomalies (Eu/Eu* = 0.5–0.8) except the sample 4LMy4-15–12 (Eu/Eu* = 1.5) (Fig. 12b). According to the content of trace elements, these rocks are subdivided into three groups (Fig. 12a). The first group (samples 4LM901 and 4LMy2/3) is distinguished by relatively low REE contents with low HREE, very high Ba (up to 1584 ppm), and positive Sr anomalies (Sr/Sr*= 2.09–2.12). The second group (samples 4LM904 and 4LMy2/9) is characterized by high U, Th, and REE, relatively low Ba (up to 614 ppm) and negative Sr anomalies (Sr/Sr*= 0.25–0.29). Pseudomorphs after white mica and quartz dominate in the first group. The second group is characterized by a significant amount of epidote-group minerals: zoisite, allanite, epidote-plagioclase pseudomorphs after zoisite, and also garnet and clinopyroxene (Fig. 6g-i). Sample 4LMy4-12-5 differs from other samples of the positive Eu anomaly (Eu/Eu* 1.5), absence of Sr anomaly, and high content of Sr, Hf, Zr and Ti (Fig. 12a, Table S2).

Gneisses that host eclogite blocks are represented by metaluminous and peraluminous TTG gneisses with variable SiO_2 content (62–72 wt%) and X_{Mg} (0.40–0.65), prevalence of Na over K ($Na_2O + K_2O$ = 6.0–8.0 wt %, Na_2O = 4.1–4.5 wt%, and K_2O = 1.5–3.9 wt%) (Fig. 11), enrichment in LREE $(La/Lu)_N$ = 9–42, and negative Eu anomaly with Eu/Eu* = 0.6–1.00 (Fig. 12). These gneisses differ significantly in composition from Ky-Grt-Ph-Qtz rocks.

5. Geochronology

5.1. U-Pb dating

Garnet-clinopyroxene-plagioclase rock, post-eclogitic mafic granulite,

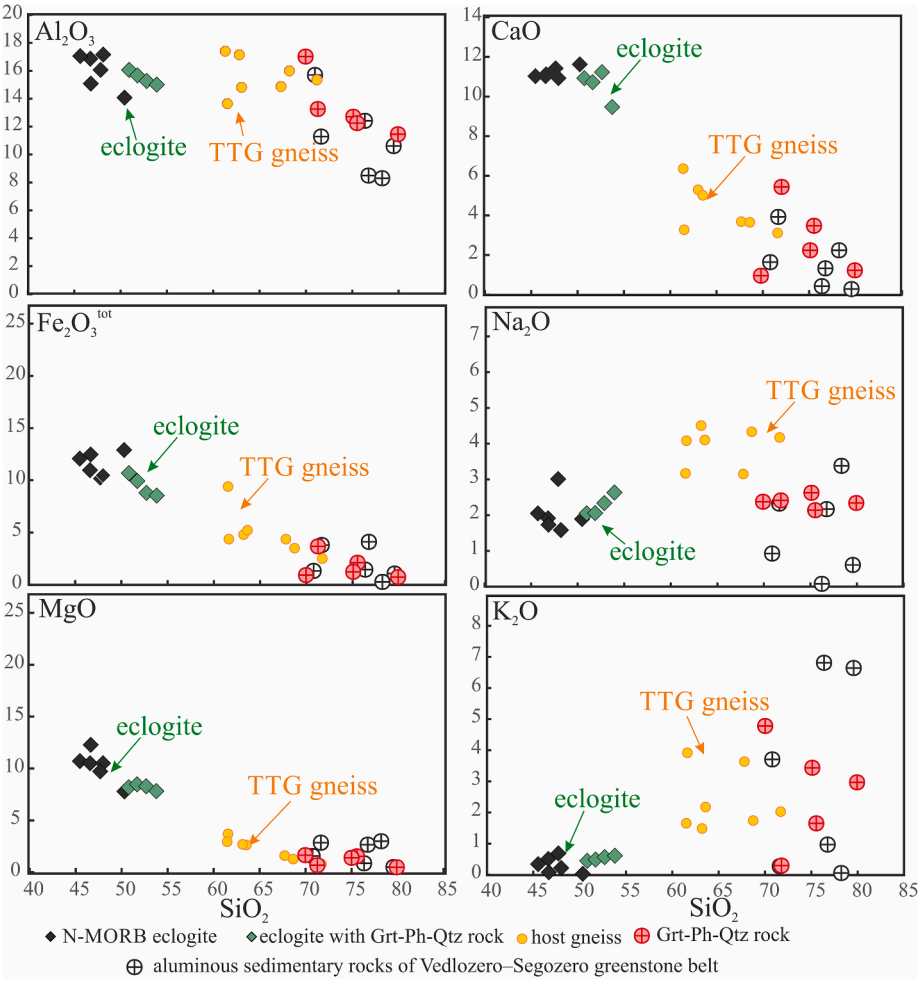

Fig. 11. Harker diagrams for metamorphic rocks from the Kuru-Vaara quarry and alumina-siliceous sedimentary rocks of the Vedlozero–Segozero greenstone belts. Chemical compositions of Ky-Grt-Ph-Qtz rocks are comparable with those of the alumina-siliceous sediment in the Vedlozero–Segozero greenstone belt after Svetova et al. (2008), Svetov and Svetova (2004).

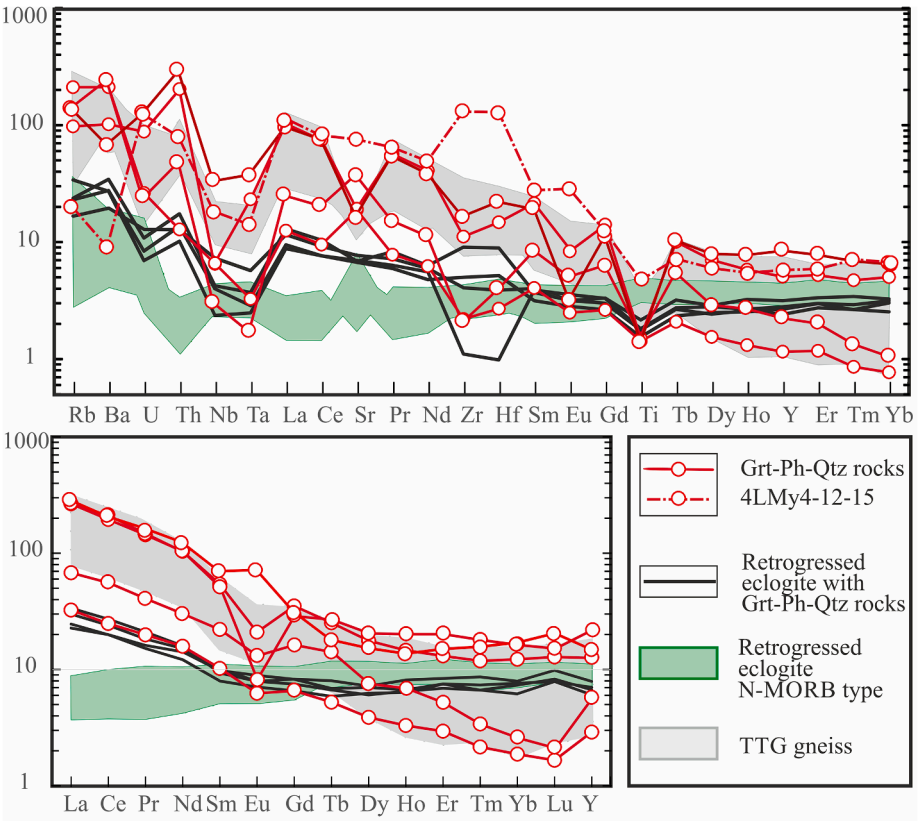

Fig. 12. Trace element composition of rocks from the Kuru-Vaara quarry normalized to the primitive mantle (Hofmann, 1988) and REE patterns of these rocks normalized to chondrite (Sun and McDonough, 1989).

sample 4LMy4-12 (Fig. 13, Table S3). Sample was taken from mafic granulite at contact with the thin vein-like body of Ky-Grt-Ph-Qtz rock (see description of the sample 4LMy4-12-5, Fig. 6b-d). Zircon in the mafic granulite contains complex split grains or grain chains with uneven rounded crystal faces (Fig. 6f). Zircon grains contain clinopyroxene, plagioclase and quartz inclusions, and display low U (23–76 ppm) and Pb (14–39 ppm). ID TIMS U-Pb zircon dating yielded the age of 2406 ± 26 Ga (n = 3, MSWD = 0.98).

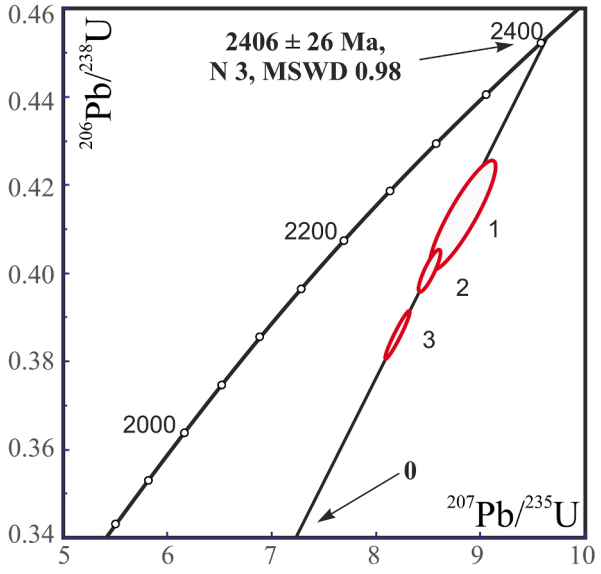

Fig. 13. U-Pb zircon Concordia diagram for the mafic granulite, sample 4LMy4-12.

5.2. *Kyanite-garnet-phengite-quartz rock*

Sample 4LMy4-12–5 (Fig. 14, Table S4) was collected from the thin vein-like fine-grained body (2–3 cm thick) within the mafic granulite 4LMy4-12. The K-feldspar deficient rock contains garnet and displays clinopyroxene and plagioclase corona between quartz and garnet (Fig. 6 e, f). Short-prismatic and isometric zircon grains, mainly homogeneous and structureless in cathodoluminescence (CL), occasionally display a core-rim structure and contain inclusions of clinopyroxene, garnet, rutile, Cl-bearing apatite, plagioclase and quartz (Fig. 14a). Zircon cores as a whole have higher Th/U ratios (0.5–1.6) and contents of Th (34–2138 ppm) and U (44–1756 ppm) than in rims (Th/U ratio 0.5–0.9, Th 20–50, U 31–61), but ages of cores and rims are similar within errors (Fig. 14a, b). Zircon from this sample was dated using LA-ICP-MS method (Fig. 14a-c). An upper intercept on the concordia diagram yields U-Pb discordant age 2444 ± 22 Ma (n = 29, MSWD = 3), the concordant age is 2429 ± 13 Ma (n = 11, MSWD = 0.09, Probability 0.76) (Fig. 14c). Only a few $^{207}Pb/^{206}Pb$ ages are Neoarchaean (Fig. 14b).

Sample 4LMy2-9 (Table S5) represents the fine-grained Ky-Grt-Ph-Qtz rock. It contains a lot of zircon grains localized within polymineralic pseudomorphs (Fig. 9c-e). Zircon grains are idiomorphic or short prismatic, cloudy, yellow-grayish with smoothed edges, and have dark CL partially metamict cores and light CL rims (Figs. 9, 14d). Cores are characterized by high Th (425–2147 ppm), U (488–1796 ppm), high Th/U ratios (0.6–1.6), elevated Hf, and contain a lot of mineral inclusions of xenotime, allanite, plagioclase and phengite (Figs. 9, 14d). Galena inclusions are within metamict areas (Fig. 9b, c). U-Pb La-ICP-MS dating of dark cores yielded the concordant age of 2468 ± 8 Ma (n = 14, MSWD = 0.11) (Fig. 14e, f). Only one grain displays $^{207}Pb/^{206}Pb$ age of about 2.0 Ga (Fig. 14e).

Sample 4LM904 (Tables S5, S6) was collected from the large Ky-Grt-

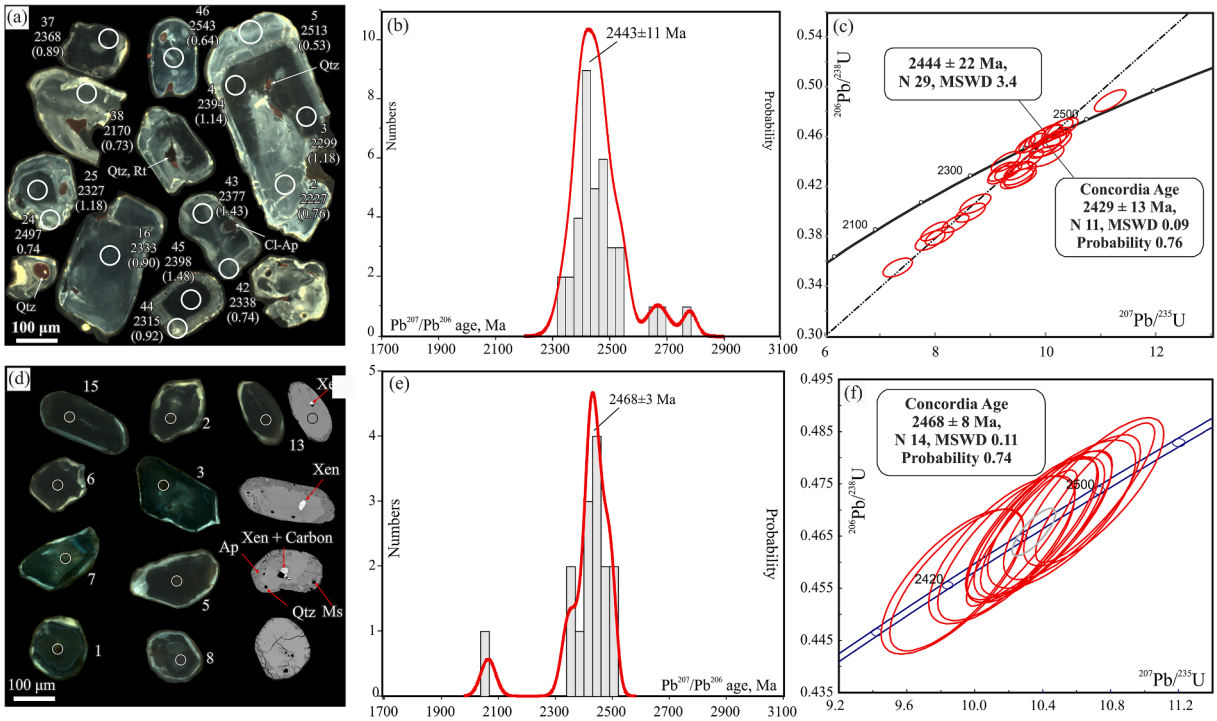

Fig. 14. Result of dating of Ky-Grt-Ph-Qtz rocks. (a-c) sample 4LMy4-12–5: (a) CL images of dated zircon; (b) Histogram of $^{207}Pb/^{206}Pb$ ages of zircon; (c) U-Pb zircon Concordia diagrams. (d-f) sample 4LMy2-9: (d) CL and BSE images of dated zircon. White circles indicate the location of LA-ICP-MS analyses; (e) Histogram of $^{207}Pb/^{206}Pb$ ages of zircon; (f) U-Pb zircon Concordia diagrams. White circles in (a) and (d) indicate the location of LA-ICP-MS analyses, digits through a slash are $^{207}Pb/^{206}Pb$ ages and Th/U ratios.

Ph-Qtz body (Fig. 5c) with abundant epidote-group minerals (zoisite, allanite, epidote), Ca-plagioclase, clinopyroxene, grossular, amphibole, and quartz (Fig. 8i). Zircon grains are idiomorphic or short prismatic, cloudy, yellow-grayish with brownish spots and relicts of oscillatory structure in transmitted light, have smoothed edges and dark in CL partially metamict cores and light rims (Fig. 15a). The metamictization of cores was apparently accompanied by a growth of the light rims. The concordant age obtained by LA-ICP-MS method for eleven points is 2428 ± 8 Ma (MSWD = 0.05) (Fig. 15b). U-Pb dating of two zircon samples by TIMS method defines the discordia with the upper intercept at 2764 ± 120 Ma and the lower intercept at 1516 ± 120 Ma (Fig. 15c, Table S6).

Trace elements composition is measured in six ~ 2.45 Ga dated places of zircon grains (Fig. 15a, point 1, 3, 4, 5, 8, 9; Table S7) (Fig. 16). The ~ 2.45 zircon displays chondrite-normalized REE pattern with positive Ce ($Ce/Ce^* = 18–870$) and negative Eu ($Eu/Eu^* = 0.1–0.8$) anomalies, HREE enrichment relative to MREE ($Lu_N/Sm_N = 8–233$) and specifically relative to LREE ($Lu_N/La_N = 30000–1150000$) (Fig. 16, Table S7). A crystallization temperature of this zircon (Ti in zircon geothermometer of Ferry and Watson (2007)) is 700–900 °C (average 783 °C) (Table S8).

Sample 4LM901 (Fig. 5e, Tables S5, S6) represents the coarse-grained Ky-Grt-Ph-Qtz rock. The short-prismatic, heterogeneous zircon that localized within polymineralic pseudomorphs displays core-rims or scrappy structures in CL. Zircon was dated by TIMS and LA-ICP-MS methods. Scrappy zircon and external rims are characterized by very low Th/U (0.15 and lower) ratios and near concordant age values of ~1.9 Ga (Fig. 17a). Cores display high Th/U (0.5–1.12) and yielded near

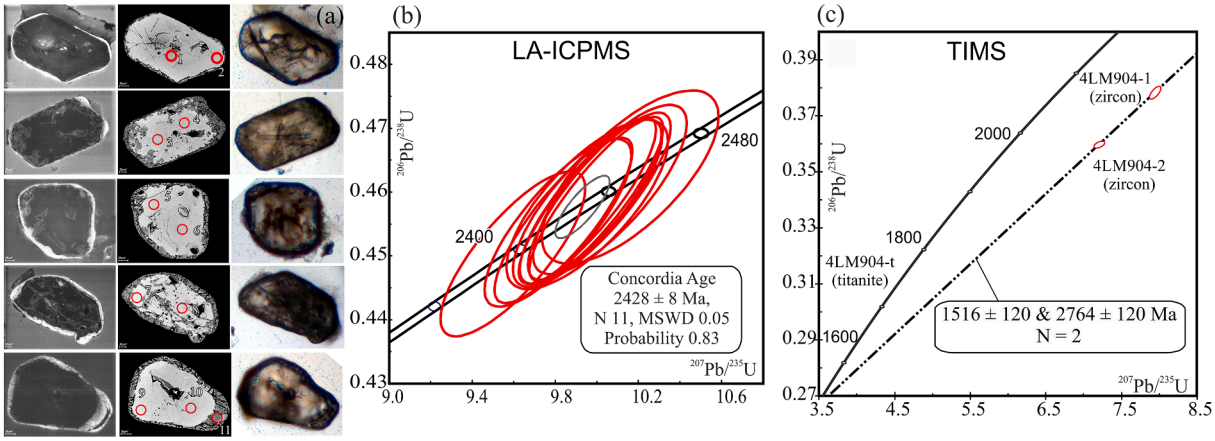

Fig. 15. Result of dating of Ky-Grt-Ph-Qtz rocks. (a) sample 4LM904: (a) CL and BSE images, and PPL photomicrographs of dated zircon. Red circles indicate the location of LA-ICP-MS analyses, digits through a slash are $^{207}Pb/^{206}Pb$ ages and Th/U ratios; (b) U-Pb zircon Concordia diagrams of zircon ages obtained by LA-ICP-MS method; (c) U-Pb zircon Concordia diagrams of zircon ages obtained by TIMS conventional method.

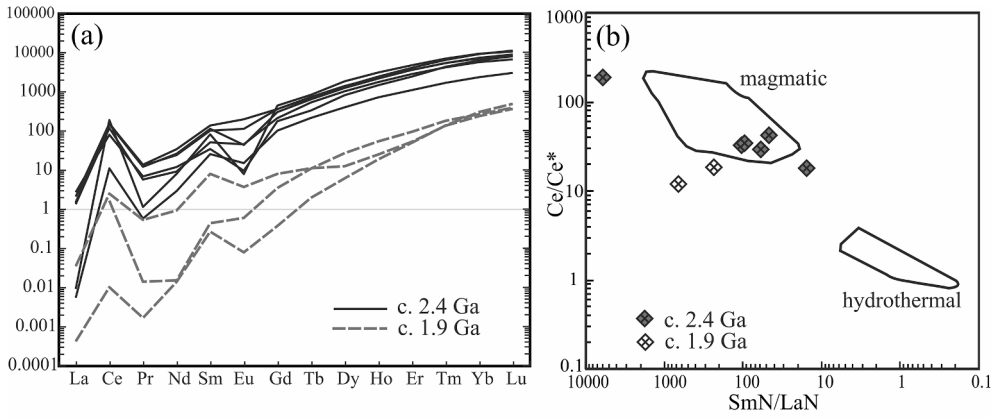

Fig. 16. (a) REE chondrite normalized patterns for the different zircon in the investigated samples. Chondrite values are from Sun and McDonough (1989); (b) Discriminant diagrams of Ce/Ce* *vs* Sm_N /La_N. Two outlined areas are defined magmatic and "hydrothermal" zircons from the Boggy Plain Zoned Pluton (Hoskin, 2005).

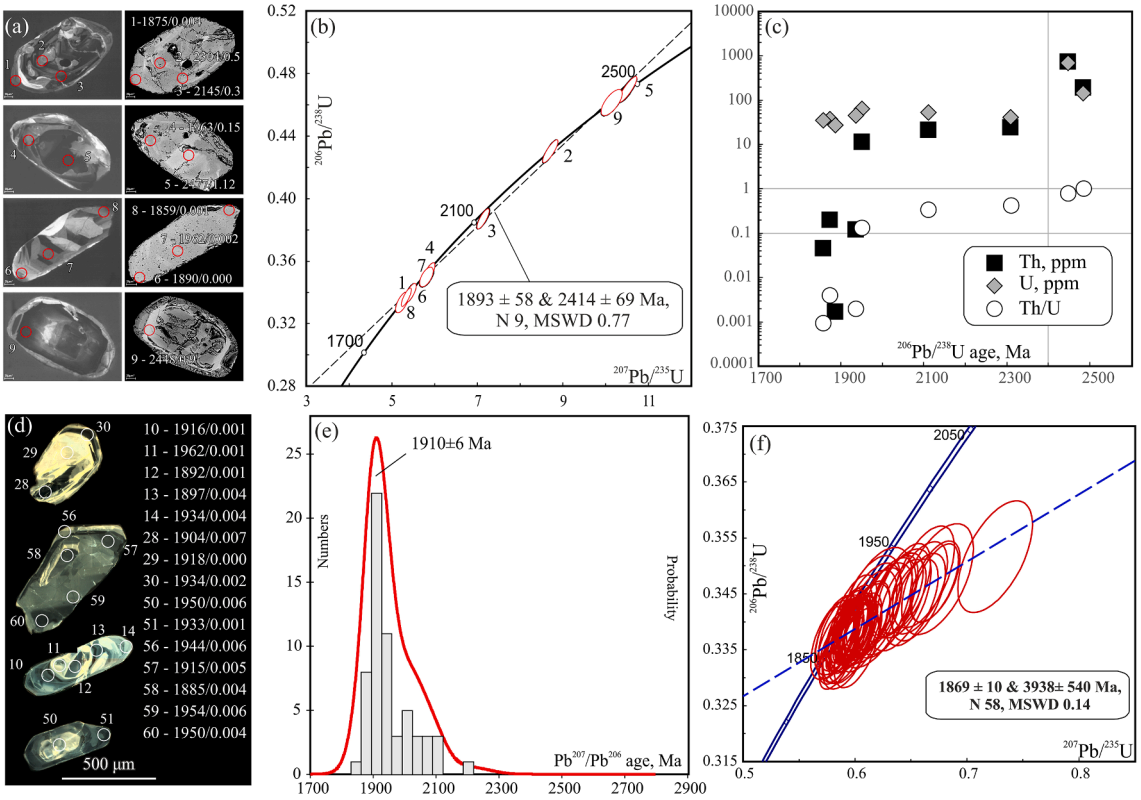

Fig. 17. Result of dating of Ky-Grt-Ph-Qtz rocks. (a-c) sample 4LM901: (a) CL and BSE images of dated zircon. (b) Concordia diagram of U-Pb zircon ages obtained by LA-ICP-MS method; (c) Th, U and Th/U ratios *vs* $^{207}Pb/^{238}U$ diagram. (d-f) Sample 4LMy2-3: (d) CL and BSE images of dated zircon. White circles indicate the location of LA-ICP-MS analyses, digits through a slash are $^{207}Pb/^{206}Pb$ ages and Th/U ratios; (e) Histogram of $^{207}Pb/^{206}Pb$ ages of zircon; (f) U-Pb zircon Concordia diagram.

concordant ages of ~2.4 Ga. Several intermediate age values were also obtained. Apparently, external rims and scrappy structures of zircon formed as a result of fluid-induced recrystallization of ~2.4 Ga zircon. Nine points define the discordia with the upper intercept at 2414 ± 69 Ma and the lower intercept at 1893 ± 58 Ma (MSWD 0.77) (Fig. 17b). This example shows how the thorium content decreases with a decrease of age values (Fig. 17c). U-Pb TIMS dating yielded a younger age 1978 ± 13 Ma (n = 2) (Table S6).

Trace elements compositions were measured in one ~ 2.45 Ga zircon core (Fig. 17a, point 5, Table S7) and three ~ 1.9 Ga zircon rims (Fig. 17a, points 4, 6, 7, Table S7) (Fig. 16). The ~ 1.9 Ga zircon is characterized by very low REE (ΣREE 73–89 ppm). The chondrite-normalized REE pattern displays low positive Ce (Ce/Ce* = 12–18) and negative Eu (Eu/Eu* = 0.3–0.5) anomalies, HREE enrichment relative to MREE (Lu_N/Sm_N = 45–1845) and specifically high HREE enrichment relative to LREE (Lu_N/La_N = 10500–1170000) (Fig. 16, Table S7). A crystallization temperature of this zircon (Ti in zircon geothermometer of Ferry and Watson (2007)) is ~ 650 °C (Table S8).

Sample 4LMy2/3 represents the coarse-grained Ky-Grt-Ph-Qtz rock (Fig. 17, Table S4). Zircon grains are clasts or cracked elongated or short-prismatic with the core-rim structure or structureless in CL (Fig. 17d). Coarse zircon fraction (≥0.5 mm) was dated by LA-ICP-MS

method. The zircon cores and rims yielded the same late Palaeoproterozoic (Orosirian) age. A weighted average $^{207}Pb/^{206}Pb$ age is ~ 1.9 Ma (n = 59, MSWD = 0.22) and has the lower intercept of the concordia at 1869 ± 10 Ma (n = 58, MSWD = 0.14) (Fig. 17e, f).

5.3. $^{40}Ar/^{39}Ar$ dating

Coarse-grained white mica grains from the *sample 4LMy2/3* and fine-grained white mica from the *sample 4LMy2/9* were dated using the $^{40}Ar/^{39}Ar$ method (Table S9). White mica in this sample represents relicts of phengitic muscovite within polymineralic pseudomorphs. $^{40}Ar/^{39}Ar$ dating of white mica yielded an age of ~ 1.7 Ga (Fig. 18).

6. The Mesoarchaean alumina-siliceous metasedimentary rocks of the Vedlozero–Segozero greenstone belts

The low-grade alumina-siliceous metapelites of the Vedlozero–Segozero greenstone belts (Fig. 5h, i) represent interpillow, lenticular or interbedded fossiliferous rocks, that are a component of the komatiite–tholeiite association (Svetov and Svetova, 2004; Svetov and Medvedev, 2013). Massive or thin-laminated sericite-quartz rocks preserve a primary sedimentary structure of flaser and lenticular bedding. Mixed-grained quartz (0.02–0.3 mm) composes microlayers (0.1–0.5 mm in thickness), discontinuous and isolated lenses (5–6 mm in size) with an admixture of feldspar and calcite are located among chlorite-bearing sericite-rich layers (Fig. 19, Table S10). The thickness of sericite-quartz beds in komatiite-basalt lavas of the Koikar area varies from 1 to 20 m (Svetov and Medvedev, 2013).

Nodular sericite-quartz schists contain a number of ovoid or lenticular shaped silica nodules flattened along schistosity (Svetov and Svetova, 2004). These nodules are 1–2 to 20 mm in size and have distinct outer contours. The nodules consist of chalcedony with albite, carbonate and contain scattered quartz phenocrysts. The nodules tightly contact with one another or are incorporated into cryptogranular silica cement with scattered sericite flakes (Svetov and Medvedev, 2013).

Volcano-sedimentary rocks underwent metamorphism under greenschist-facies conditions. Volcanic glass of mafic lavas replaced by chlorite; olivine phenocrysts replaced by iddingsite; pseudomorphic replacement of the pyroxene phenocrysts by uralite is usual, plagioclase glomerocrysts are saussuritized; vesicle-filled chalcedony began to recrystallize into microgranular quartz aggregate. In the alumina-siliceous sediments, sericite flakes are enlarged along of boundaries of quartz layers and lenses, and quartz grains coarsened and get granoblastic structure within the layers and lenses.

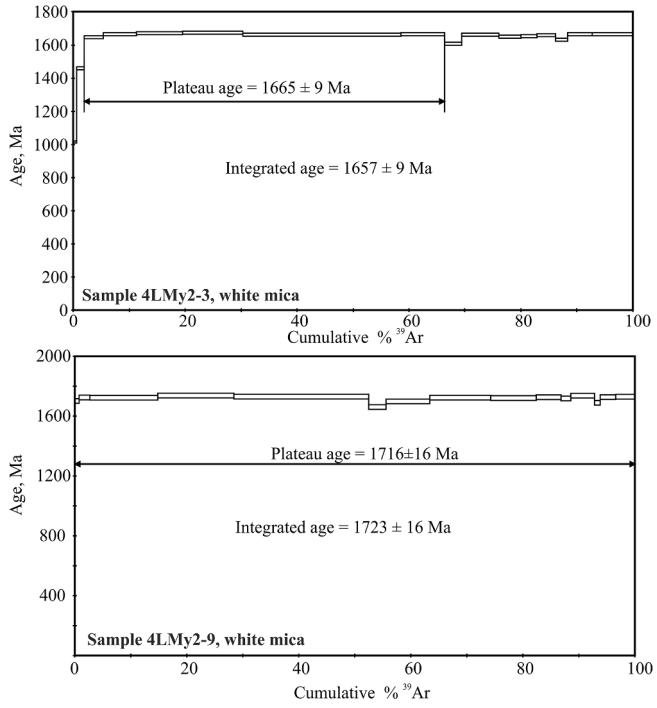

Fig. 18. $^{40}Ar/^{39}Ar$ data on white mica.

The major-element composition of the alumina-siliceous rocks is variable (wt %): 75.20–86.23 SiO_2, 0.03–0.42 TiO_2, 8.10–11.41 Al_2O_3, 0.14–1.52 Fe_2O_3, 0.10–0.36 FeO, 0.01–0.05 MnO, 0.17–0.57 MgO, 0.14–0.98 CaO, 0.50–2.10 Na_2O, 3.15–4.47 K_2O, 0.06–0.22 H_2O; LOI is 0.30–1.72 (Fig. 12). The rocks are markedly enriched (ppm) in Rb (400–720), Ba (700–1200), and REE (Svetova et al., 2008, Svetov and Svetova, 2004).

7. Discussion

7.1. Origin of Ky-Grt-Ph-Qtz rock

Initially, we discussed two hypotheses the origin of Ky-Grt-Ph-Qtz rocks (Dokukina et al., 2017). Ky-Grt-Ph-Qtz rocks have sedimentary protolith (1) or are a result of dehydration or partial melting of the hydrated upper part of an oceanic slab that descended into a subduction zone (2). New data make it possible to return to the discussion of this problem.

Both sediments and hydrothermally altered under submarine conditions oceanic volcanic rocks could be sources of elevated concentration of water, boron, and barium (Ryan and Langmuir, 1993; Plank and Langmuir, 1998 and references therein) that are necessary for formation of granitic melts, chemical composition of which corresponds to Ky-Grt-Ph-Qtz rocks. The veins could be solidified felsic melts produced by dehydration melting of boron-bearing rocks under high-pressure conditions of subduction zone or conversely of decompression melting of these rocks during ascent. Barium is considered to be highly "fluid mobile" and high Ba/La ratios in Ky-Grt-Ph-Qtz rocks can arise from addition of aqueous fluid from the slab (Elliott et al., 1997; Pearce et al., 2005). However high Th/Nb ratios in Ky-Grt-Ph-Qtz rocks suggest that sediment melting has occurred (Elliott et al., 1997; Johnson and Plank, 1999). Now we have more evidence for the sedimentary protolith model.

The low-grade sericite-quartz schist of the Vedlozero–Segozero greenstone bands may be interpreted as analogues of the Ky-Grt-Ph-Qtz rocks of the Salma eclogite association. The relationship between the Ky-Grt-Ph-Qtz rock and eclogite (Fig. 5a) resembles pillow lavas with an interpillow space filled sedimentary material (Fig. 5h).

The chemical composition of the Ky-Grt-Ph-Qtz rocks is quite comparable to alumina-siliceous sediments in the Vedlozero–Segozero greenstone belt (Figs. 11, 19). Thus, we consider that the alumina-siliceous metasedimentary rocks with sericite-quartz assemblages are low-grade analogues of Ky-Grt-Ph-Qtz rocks.

According to Svetov and Medvedev (2013), Mesoarchaean alumina-siliceous sediments formed by a chemical deposition of silica from metastable colloidal solutions formed in subaqueous hydrothermal systems. Yet flaser and lenticular bedding structures are commonly created at alternating sand and mud layers when terrigenous sediment is exposed to intermittent flows (Martin, 2000). It may be evidence of shallow clastic and clay material in the alumina-siliceous sediments of the Vedlozero–Segozero greenstone belts.

The genetic interpretation for the Ky-Grt-Ph-Qtz rocks as initially sedimentary deposit explains the structure of those rocks, unusually composition and its variations, as well as occurrence of compositional heterogeneity (Fig. 7h-i). The augen structure of Ky-Grt-Ph-Qtz rocks can be inherited lenticular structure of the primary sedimentary rock. If this interpretation is valid, the Ky-Grt-Ph-Qtz rocks (Fig. 5b-h) are probably high-pressure equivalents of interbeds of sericite–quartz sedimentary rocks between lava flows or basaltic pyroclastic rocks. Thus, protolith of eclogite assemblages, that contains the Ky-Grt-Ph-Qtz rocks,

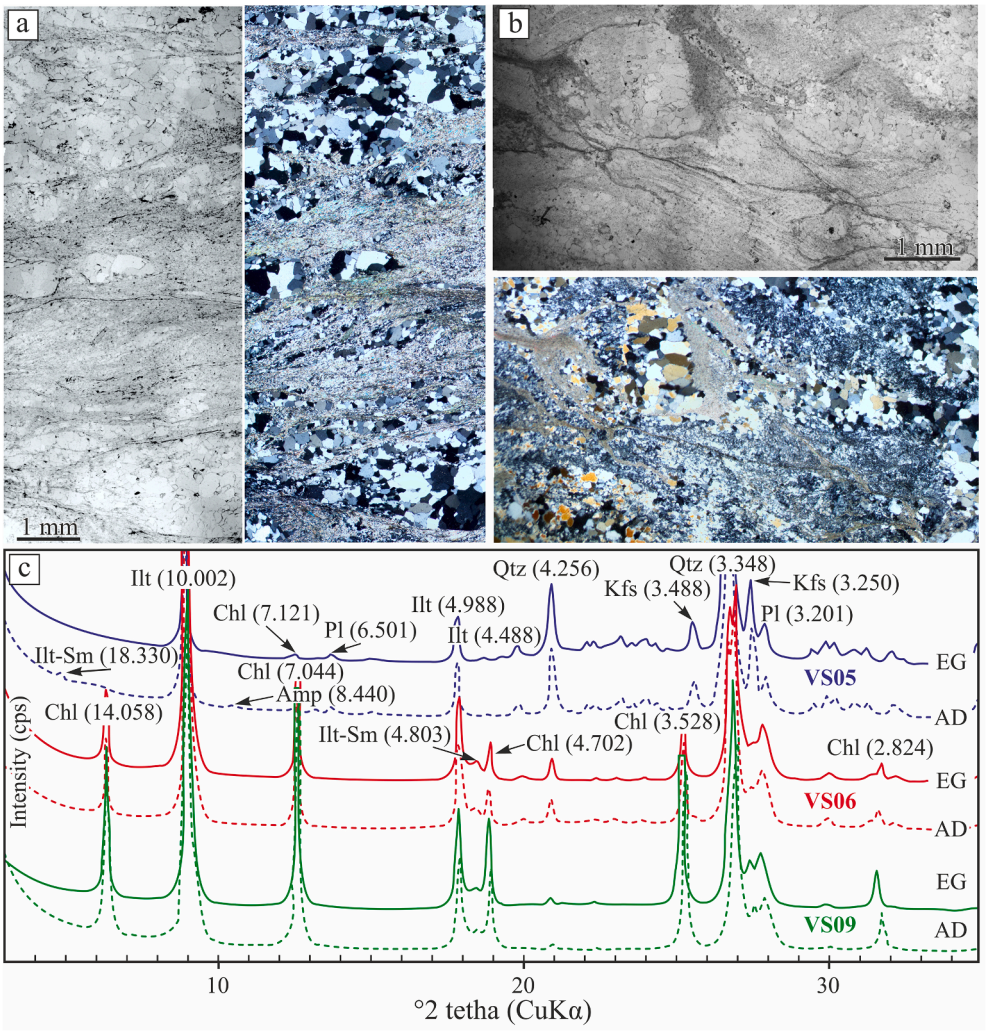

Fig. 19. (a, b) PPL and XPL photomicrographs of flaser and lenticular structures of Mesoarchaean sericite-quartz sedimentary rocks in the Koikar structure of the Vedlozero–Segozero greenstone belts. The cryptocrystalline quartz partially underwent recrystallization with forming of the quartz granoblastic aggregate. (a) Sample VS05; (b) Sample VS06 was taken from the outcrop shown in Fig. 5i. (c) The oriented X-ray diffraction patterns of the clay fraction < 2 μm of the samples VS05, VS06 and VS09. AD – air-dried, EG – ethylene glycol saturated. Chl – chlorite, Ilt – illite, Qtz – quartz, Kfs – K feldspar, Pl – plagioclase.

can be compared with volcanic and sedimentary rocks including pillow lavas erupted under submarine conditions; sediments mark breaks in volcanic activity. Fluid inclusions trapped in large relic quartz grains of Ky-Grt-Ph-Qtz rocks yielded an isochore that corresponds to a high-temperature and low-pressure flat geothermal gradient (~50 °C/km).

7.2. *Polymineral pseudomorphs: phengite + quartz melting*

Previous experiments on the melting of quartz + phengite show that polymineralic pseudomorphs consisting of biotite, K-feldspar, and aluminosilicates replace phengite monocrystals (Brearley and Rubie, 1990; Thompson, 1982; Vielzeuf and Holloway, 1988). In the kyanite zone, the dehydration melting of Ti-rich phengite with quartz is described by the following incongruent melting reactions: Ph + Qtz → Ky + Kfs + Bt + Rt + melt and Ph + Qtz → Ky + Kfs + Grt + Rt + melt. The experimental results reproducing melting and disequilibrium breakdown of muscovite + quartz in H_2O-saturated and H_2O-unsaturated conditions show that these pseudomorphs formed on the site of phengite monocrystals (Brearley and Rubie, 1990).

By analogy with the experiments, it is suggested that zoned feldspar moats in the Ky-Grt-Ph-Qtz rocks are formed as products of phengite mica fusion and reflect evolution of the melt. The appearance of K-feldspar as a product of the reaction is evidence for water-undersaturation because this mineral did not form in water-saturated experiments (Brearley and Rubie, 1990, Hermann and Green, 2001).

Platelets and needles of kyanite and dumortierite are found along cleavage planes in mica in the pseudomorphs after phengite in the Ky-Grt-Ph-Qtz rocks. A minor amount of dumortierite in pseudomorphs is consistent with the occurrence of boromuscovite as a component of initial phengite (Korhonen and Stout, 2005; Jung and Schreyer, 2002).

The appearance of corundum in rocks with abundant free quartz is an unusual phenomenon mostly related to ultrahigh-temperature metamorphism (Kelsey, 2008). However, corundum occurs only within pseudomorphs and is never in contact with quartz. The quartz-undersaturated mineral assemblage that consists of muscovite, K-feldspar, biotite, plagioclase, and corundum, is consistent with dehydration reaction Ph = Crn + Kfs + Bt + melt. The melt is practically not removed from the place of its generation probably owing to the armoring effect of the host quartz. Feldspar of different compositions (K-feldspar, albite, oligoclase, and mesoperthites) was formed due to crystallization of the melt and following subsolidus recrystallization during slow cooling of anatectic rocks (Dokukina et al., 2017).

7.3. *Metamorphic conditions*

PT path was reconstructed for Ky-Grt-Ph-Qtz rocks and the host eclogite in the Kuru-Vaara quarry (Fig. 20) (Dokukina et al., 2017). As a result of eclogite-facies metamorphism, the alumina-siliceous metasediments and mafic rocks, respectively, have been transformed into the Ky-Grt-Ph-Qtz rocks and Grt-Omp eclogites under a pressure no lower than 21 kbar and at a temperature of ~ 650 °C. During a transfer to the upper crust under conditions of high-pressure granulite facies

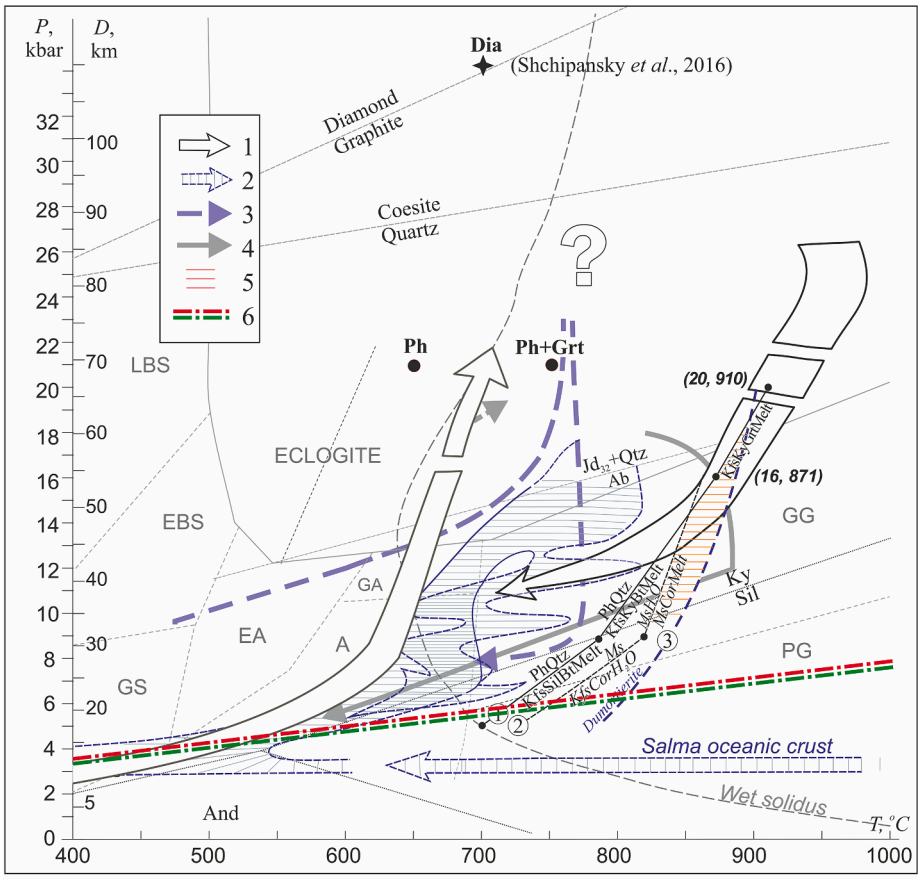

Fig. 20. Reconstruction of *PT*-paths of studied rocks (modified from Dokukina et al., 2017). 1 – Possible *PT* paths of Ky-Grt-Ph-Qtz rock and host eclogite after Dokukina et al. (2017); 2 – *PT*-paths of metamorphic evolution of the Salma eclogite association after Mints et al. (2014); 3 – *PT*-paths of the metamorphic evolution of the Kuru-Vaara eclogites after Shchipansky et al. (2012) ; 4 – *PT*-paths of the metamorphic evolution of the Kuru-Vaara eclogites after Liu et al. (2017); 5 – stability field of pseudomorph mineral assemblage; 6 - calculated isochores of CO_2 fluid inclusions (this work). Numbers in circles are relevant phengite reactions: 1 – under water-undersaturated conditions after Thompson (1982), Vielzeuf and Holloway (1988); 2 – water-saturated conditions after Brearley and Rubie (1990) and references therein; 3 – stability fields of dumortierite, after Schreyer and Werding (1997).

metamorphism, phengite underwent incongruent melting with the formation of complex polymineralic pseudomorphs that consist of feldspars, biotite, muscovite, kyanite and also contain corundum and dumortierite. The peak of high-temperature metamorphism during partial melting is estimated at 850–900 °C. The crystallization conditions for reintegrated primary feldspar deduced from mesoperthites provide evidence for a probable reaching of ultrahigh temperature (~1000 °C) of the feldspar crystallization from melt. The lower pressure and temperature limit (~8.6 kbar and 770 °C, respectively) corresponds to melting of pure muscovite + quartz under water-undersaturated conditions. The invariant point at 16 kbar and 871 °C (Fig. 20) is the upper limit of pressure and temperature for the stable K-feldspar–kyanite–phlogopite assemblage. Garnet is stable at higher *P* and *T*, and its occurrence within the pseudomorphs indicates phengite melting under pressures above 16 kbar.

If the Ky-Grt-Ph-Qtz rock was formed after metasediments and pillow lava was the protolith of eclogite, subduction started from the level of a seafloor. We supposed white mica and quartz forming was synchronous during subduction of alumina-siliceous sediment, hence primary CO_2-rich fluid inclusions were trapped during forming of high-pressure metamorphic mineral assemblage. The isochore slope (Fig. 10f) coincides with the *PT*-path of Salma rocks in the low-pressure field at beginning of oceanic rocks subduction or with the final stage of exhumation to shallow level (Fig. 20). In the latter case, the decomposition of quartz would lead not only to fluid inclusions capturing by quartz but also to phengite alteration. Thus, the isochore obtained at studies of fluid inclusions in quartz evidently yields *PT*-path corresponding to a beginning of subduction of the Salma oceanic rocks (Figs. 10f, 20).

7.4. Age of melting

U-Pb dating of Ky-Grt-Ph-Qtz rocks yielded two main age values of ~ 2.45 and ~ 1.9 Ga and some more ancient dates in the samples 4LMy4-12-5 and 4LM904. This result is quite unexpected since the host eclogites (according to previous studies) contain abundant Mesoarchaean and Neoarchaean zircons (Fig. 21).

The Early Palaeoproterozoic (~2.45 Ga) zircon in Ky-Grt-Ph-Qtz rocks displays no CL emission that is characteristic of the high content of radioactive elements. The radioactive decay of U and Th and their unstable daughter nuclei damages the zircon structure. This radiation damage, in turn, leads to a drastic decrease in CL intensity (Ewing et al., 2003; Nasdala et al., 2003). Despite clear signs of metamictization, zircon grains retain relicts of oscillatory zoning (see Fig. 15a, upper grain). The REE patterns and high Th/U ratios in the Palaeoproterozoic (~2.45 Ga) zircons are very similar to igneous zircons (Figs. 16, 21) (Hoskin and Schaltegger, 2003; Rubatto, 2002).

The ~ 2.45 Ga zircon is localized in areas of phengite + quartz melting and contains white mica and garnet inclusions (Fig. 10) suggesting that zircon grew from partial melt after formation of the pyrope garnet + kyanite + phengite + quartz eclogite-facies mineral assemblage. Average crystallization temperatures of these zircons are 780 °C (Table S8), which is a little less than the estimated temperatures of granulite-facies metamorphism and partial melting conditions (850–900 °C).

Zircon ages do not usually correspond to the peak of high-temperature metamorphism but instead provide information on the history of cooling from high temperatures, including the time and rates of exhumation of the deep roots of mountain chains (Harley et al., 2007). At ~ 2.45 Ga, the granulite-facies temperature was enough high for total dissolution of finer pre-existing zircon and release of zirconium and radioactive elements to the partial melt. When the rocks cooled down towards solidus, any melts that have not been extracted from them will crystallize (Sawyer, 2001; Harley, 2004). At temperatures in the range of 750–650 °C, this led to the production of fluid that interacted with and

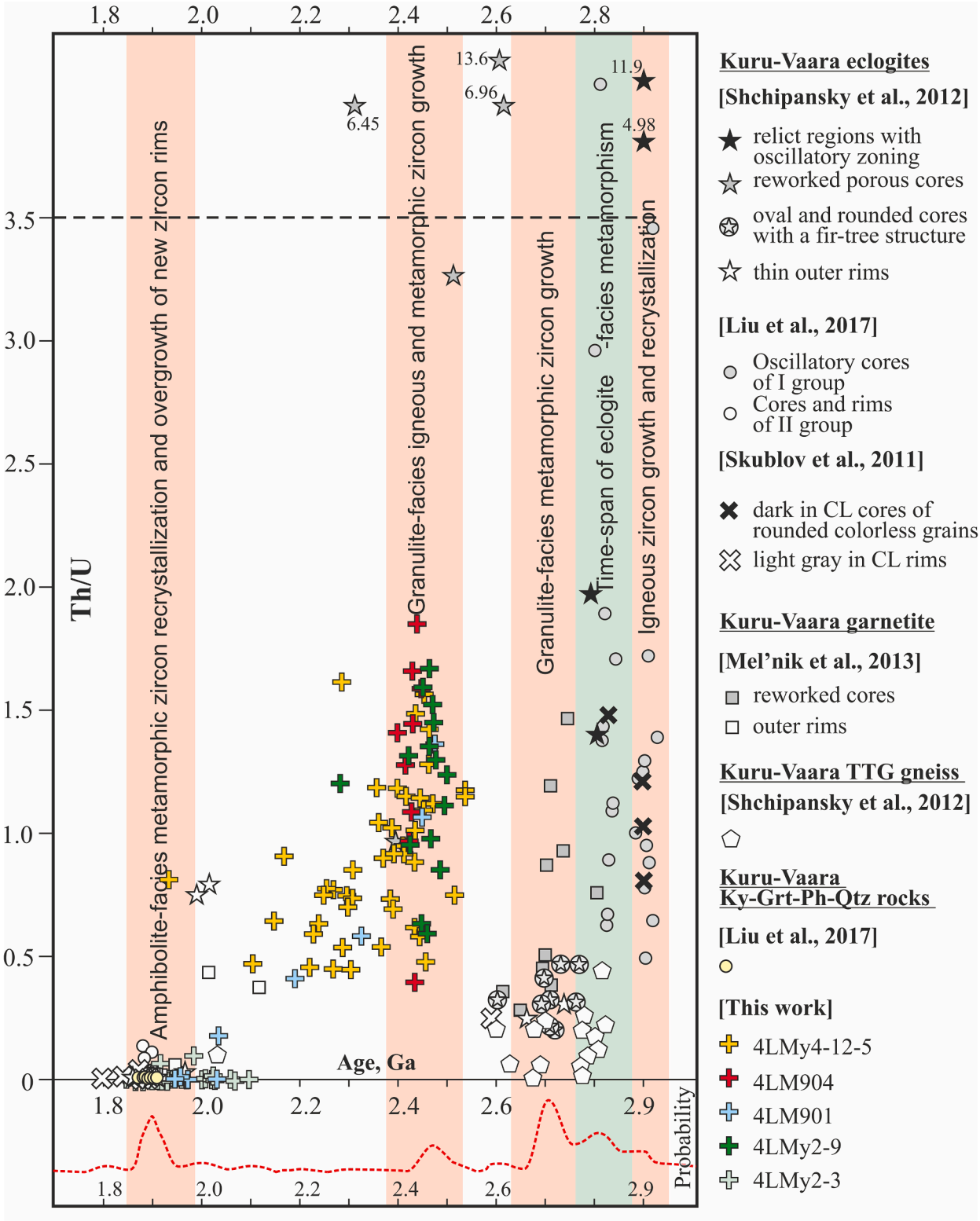

Fig. 21. Integrated age (Ga) *vs* Th/U ratio diagrams from dated rocks of the Kuru-Vaara quarry.

partially hydrate the previously equilibrated high-T mineral assemblages. Hydration reactions associated with final melt crystallization and released of water promoted growth of new zircon. Also, new zircon could grow as a result of Zr-liberating reactions: garnet breakdown (Figs. 7b, 8i) and rutile, allanite and xenotime decomposition (Figs. 9, 14a, d). Furthermore, the fluids could also attack pre-existing zircon, recrystallizing susceptible zones (Vavra et al., 1999, Geisler et al., 2007), leaching trace elements from zircon surfaces (Carson et al., 2002), causing recrystallization of old undissolved zircon and resetting the U–Pb systematics.

Zircon grains in the mafic granulite are split and display pole-like, rounded and amoeba-like (Fig. 6f) shapes, representing evidence of zircon growth in solid rock in limited-growth conditions. The Early Palaeoproterozoic U-Pb age (~2.4 Ga) of zircon in the mafic granulite,

sample 4LMy4-12, agrees well with U-Pb ages of Ky-Grt-Ph-Qtz rocks.

During the late Palaeoproterozoic (~1.8–1.9 Ga), the zircon underwent recrystallization. Variable amounts of Zr, REE, U, Th and Pb removed from zircon into fluid; thorite, uraninite, galenite inclusions and separate Th-, U- and REE-rich minerals outside zircon formed (Fig. 9) and dissolution-reprecipitation processes made metamorphic overgrowths of new zircon rims due to high-radioactive Early Palaeoproterozoic cores. $^{40}Ar/^{39}Ar$ dating of white mica in the kyanite-garnet-phengite-quartz rock yields time of the system cooling to 300–280 °C (Harrison et al., 2009) at ~ 1.7 Ga.

7.5. Tectonic implication

A comparison of the tectonothermal evolution of the Salma eclogite association with the geological history of the Kola-Karelia region demonstrates a good coherence. (Fig. 2). The new petrological and geochronological data are the important arguments of the Archaean age of eclogite-facies metamorphism. The Early Palaeoproterozoic ~ 2.4 Ga mantle upwelling originated a large igneous province with gabbro-anorthosite, layered mafic–ultramafic and charnockite magmatism, and bimodal volcanism (Sharkov, 2006; Stepanova and Stepanov, 2010; Stepanova et al., 2014, 2015; Erofeeva et al., 2019), and additional heating of the Belomorian rocks right up to ultrahigh-temperature conditions, partial melting of metapelitic rocks and appearance of the granulite facies mineral assemblage in mafic rocks (Mints et al., 2015 and references therein). Moreover, the late Palaeoproterozoic ~ 1.9 Ga tectonothermal event in the Belomorian Eclogite Province caused uplift of high-pressure rocks from lower crust with formation of amphibolite facies mineral assemblages.

8. Conclusions

The results obtained substantially supplement the former evolutionary model of the Belomorian Eclogite Province. Protoliths of the eclogite facies rocks in the Belomorian Eclogite Province were the components of the Mesoarchaean oceanic crust. Volcanic rocks including pillow lavas erupted under submarine conditions presented in this paper were one of the important components of this crust. The sediments mark breaks in volcanic activity. As a result of eclogite-facies metamorphism, the alumina-siliceous sediments have been transformed into kyanite-garnet–phengite–quartz rocks. In the Early Palaeoproterozoic at ~ 2.45 Ga, eclogite-facies metasedimentary rocks underwent partial melting and disequilibrium breakdown of phengite + quartz. The minimum melting temperature was 850–900 °C in the wide pressure range of 9–16 kbar.

New data display the important role of sedimentary material in the formation of leucocratic felsic rocks in subduction zone. Finally, the obtained results show that the younger mantle-plume processes made a substantial contribution to creation of the Belomorian Eclogite Province's final appearance.

CRediT authorship contribution statement

Ksenia Dokukina: Conceptualization, Methodology, Investigation, Formal analysis, Validation, Writing - original draft, Writing - review & editing, Visualization. **M.V. Mints:** Conceptualization, Methodology, Writing - review & editing, Visualization. **V.B. Khubanov:** Investigation, Formal analysis. **V.S. Sheshukov:** Investigation, Formal analysis. **A.N. Konilov:** Investigation, Formal analysis. **T.B. Bayanova:** Investigation, Formal analysis. **T.V. Kaulina:** Investigation, Formal analysis. **M.A. Golunova:** Investigation, Formal analysis. **P.A. Dokukin:** Funding acquisition, Writing - review & editing. **O.I. Okina:** Investigation, Formal analysis. **K.V. Van:** Resources. **D.S. Yudin:** Investigation, Formal analysis. **A.V. Travin:** Resources, Investigation. **A.V. Zaitsev:** Investigation, Formal analysis. **V.L. Kosorukov:** Resources, Formal analysis. **V.I. Pozhilenko:** Visualization. **T.I. Golovanova:** Resources.

Declaration of Competing Interest

The authors declare that they have no known competing financial interests or personal relationships that could have appeared to influence the work reported in this paper.

Acknowledgments

The study was being carried out following the plans of the scientific research of the Geological Institute of RAS (project no. 0120145918) and was supported by the Russian Foundation for Basic Research (project no. 20-05-00190). The U-Pb isotopic LA-ICP-MS study was partially performed in the Analytical Centre of Mineralogical, Geochemical and Isotope Studies" in the Geological Institute, SB RAS Ulan-Ude, Russia (government task project No AAAA-A16-116122110027-2). This paper has been supported by the RUDN University Strategic Academic Leadership Program. $^{40}Ar/^{39}Ar$ dating is done on state assignment of IGM SB RAS. Anonymous reviewers improved significantly the first, second and third versions of the manuscript. We thank reviewers for their constructive review and for assistance with the English that improved the presentation.

Appendix A. Supplementary data

Supplementary data to this article can be found online at https://doi.org/10.1016/j.precamres.2021.106260.

References

Aranovich, L.Y., Bortnikov, N.S., Zinger, T.F., Borisovskiy, S.E., Matrenichev, V.A., Pertsev, A.N., Sharkov, E.V., Skolotnev, S.G., 2017. Morphology and impurity elements of zircon in the oceanic lithosphere at the Mid-Atlantic Ridge axial zone (6–13° N): Evidence of specifics of magmatic crystallization and postmagmatic transformations. Petrology 25 (4), 339–364. https://doi.org/10.1134/S0869591117040026.

Baksi, A.K., Archibald, D.A., Farrar, E., 1996. Intercalibration of 40Ar/39Ar dating standards. Chem. Geol. 129, 307–324.

Balagansky, V., Shchipansky, A., Slabunov, A., Gorbunov, I., Mudruk, S., Sidorov, M., Azimov, P., Egorova, S., Stepanova, A., Voloshin, A., 2015. Archean Kuru-Vaara eclogites in the northern Belomorian Province, Fennoscandian Shield: crustal architecture, timing and tectonic implications. Int. Geol. Rev. 57, 1543–1565.

Bibikova, E.V., Slabunov, A.I., Bogdanova, A.I., Skiöld, T., Stepanov, V.S., Borisova, E.Yu, 1999. Early magmatism of the Belomorian Mobile Belt, Baltic Shield: lateral zoning and isotopic age. Petrology 7 (2), 123–146.

Brearley, A.J., Rubie, D.C., 1990. Effects of H2O on the disequilibrium breakdown of muscovite + quartz. J. Petrol. 31, 925–956.

Carson, C.J., Ague, J.J., Grove, M., Coath, C.D., Harrison, T.M., 2002. U-Pb isotopic behavior of zircon during upper-amphibolite facies fluid infiltration in the Napier Complex, east Antarctica. Earth Planet. Sci. Lett. 199, 287–310.

Corfu, F., Hanchar, J.M., Hoskin, P.W.O., & Kinny, P., 2003. Atlas of Zircon Textures. In: Hanchar JM, Hoskin PWO (ed) Zircon: in Review in Mineralogy and Geochemistry, 53, 469–500.

Dick, H.J.B., Natland, J.H., Alt, J.C., Bach, W., Bideau, D., Gee, J.S., Haggas, S., Hertogen, J.G.H., Hirth, G., Holm, P.M., Ildefonse, B., Iturrino, G.J., John, B.E., Kelley, D.S., Kikawa, E., Kingdon, A., LeRoux, P.J., Maeda, J., Meyer, P.S., Miller, D. J., Naslund, H.R., Niu, Y.-L., Robinson, P.T., Snow, J., Stephen, R.A., Trimby, P.W., Worm, H.-U., & Yoshinobu, A., 2000. A long in situ section of the lower ocean crust: results of ODP Leg 176 drilling at the Southwest Indian Ridge. Earth and Planetary Science Letters, 179, 31–51.

Dokukina K.A. 2017. Granite melts forming in high-pressure conditions (Belomorian eclogite province, Eastern Fennoscandian Shield). GeoScience, 23, 10-27 (in Russian). https://www.elibrary.ru/item.asp?id=30034985.

Dokukina, K.A., & Konilov, A.N., 2011. Metamorphic evolution of the Gridino mafic dyke swarm (Belomorian eclogite province, Russia). In: Ultrahigh-Pressure Metamorphism. 5 Years After the Discovery of Coesite and Diamond (eds Dobrzhinetskaya, L.F., Faryad, S.W., & Wallis, S.), pp. 579–621. Elsevier.

Dokukina, K.A., Bayanova, T.B., Kaulina, T.V., Travin, V.V., Mints, M.V., Konilov, A.N., Serov, P.A., 2012. The Belomorian eclogite province: the sequence of events and the age of magmatic and metamorphic rocks of the Gridino eclogite association. Russ. Geol. Geophys. 53, 1023–1054.

Dokukina, K.A., Bayanova, T.B., Travin, A.V., Kaulina, T.V., Konilov, A.N., 2010. New geochronological data for metamorphic and magmatic rocks of the Belomorian eclogites province (Gridino Area, Northern Karelia). Doklady Earth Sci. 432 (1), 671–676.

Dokukina, K.A., Kaulina, T.V., Konilov, A.N., 2009. Dating of key events in the Precambrian polystage complexes: an example from Archean Belomorian Eclogite Province, Russia. Doklady Earth Sci. 425 (2), 296–301.

Dokukina, K.A., Konilov, A.N., Kaulina, T.V., Mints, M.V., Van, K.V., Natapov, L.M., Belousova, E.A., Simakin, S.G., Lepekhina, E.N., 2014. Archean to Palaeoproterozoic high-grade evolution of the Belomorian Eclogite Province in Fennoscandian Shield (Gridino area): geochronological evidences. Gondwana Res. 25, 585–613.

Dokukina, K.A., Konilov, A.N., Mints, M.V., Belousova, E.A., Dokukin, P.A., Kaulina, T. V., Natapov, L.M., & Van, K.V., 2015. Mesoarchean–Neoarchean Belomorian Eclogite Province. In: East European Craton: Early Precambrian history and 3D models of deep crustal structure, (eds Condie K. & Harvey F. E.), Boulder, Colorado, Geological Society of America Special Paper, Vol. 510, pp. 56-88.

Dokukina, K., Mints, M., 2019. Subduction of the Mesoarchean spreading ridge and related metamorphism, magmatism and deformation by the example of the Gridino eclogitized mafic dyke swarm, the Belomorian Eclogite Province, eastern Fennoscandian Shield. J. Geodyn. 123, 1–37.

Dokukina, K.A., Mints, M.V., Konilov, A.N., 2017. Melting of eclogite facies sedimentary rocks in the Belomorian Eclogite Province, Russia. J. Metamorph. Geol. 35, 435–451. https://doi.org/10.1111/jmg.12239.

Dokukina K.A., Mints M.V., Konilov A.N., Sheshukov V.S., Khubanov V.B., Bayanova T. B., Van K.V., & Golovanova T.I., 2020. Palaeoproterozoic granulite-facies metamorphism at ~ 2.4 Ga in rocks of the Belomorian eclogite province, Fennoscandian Shield, Russia. GeoScience, 2, 4-23 (in Russian). https://www.elibrary.ru/item.asp?id=43851919.

Elkins, L.T., Grove, T.L., 1990. Ternary feldspar experiments and thermodynamic models. Am. Mineral. 75, 544–559.

Elliott, T., Plank, T., Zindler, A., White, W., Bourdon, B., 1997. Element transport from slab to volcanic front at the Mariana arc. J. Geophys. Res. 102, 14991–15019.

Erofeeva, K.G., Stepanova, A.V., Samsonov, A.V., Larionova, YuO., Egorova, S.V., Arzamastsev, A.A., Kovalchuk, E.V., 2019. 2.4 Ga Mafic Dikes and Sills of Northern Fennoscandia: Petrology and Crustal Evolution. Petrology 27 (1), 17–42.

Ewing, R.C., Meldrum, A., Wang, L.M., Weber, W.J., Corrales, L.R., 2003. Radiation effects in zircon. Rev. Mineral. Geochem. 53, 387–425.

Ferry, J.M., Watson, E.B., 2007. New thermodynamic models and revised calibrations for the Ti-in-zircon and Zr-in-rutile thermometers. Contrib. Miner. Petrol. 154, 429–437.

Geisler, T., Schaltegger, U., Tomaschek, F., 2007. Re-equilibration of zircon in aqueous fluids and melts. Elements 3, 43–50.

Grimes, C.B., John, B.E., Cheadle, M.J., Mazdab, F.K., Wooden, J.L., Swapp, S., Schwartz, J.J., 2009. On the occurrence, trace element geochemistry, and crystallization history of zircon from in situ ocean lithosphere. Contrib. Miner. Petrol. 158 (6), 757–783. https://doi.org/10.1007/s00410-009-0409-2.

Grimes, C.B., John, B.E., Cheadle, M.J., Wooden, J.L., 2008. Protracted construction of gabbroic crust at a slow spreading ridge: Constraints from 206Pb/238U zircon ages from Atlantis Massif and IODP Hole U1309D (30°N, MAR). Geochem. Geophys. Geosyst. 9 (8), Q08012. https://doi.org/10.1029/2008gc002063.

Groppo, C., Lombardo, B., Rolfo, F., Pertusati, P., 2007. Clockwise exhumation path of granulitized eclogites from the Ama Drime range (Eastern Himalayas). J. Metamorph. Geol. 25, 51–75.

Harley, S.L., 2004. Extending our understanding of Ultrahigh temperature crustal metamorphism. J. Mineral. Petrol. Sci. 99, 140–158.

Harley, S.L., Kelly, N.M., Möller, A., 2007. Zircon behaviour and the thermal histories of mountain chains. Elements 3, 25–30.

Harrison, T.M., Célérier, J., Aikman, A.B., Hermann, J., Heizler, M.T., 2009. Diffusion of 40Ar in muscovite. Geochim. Cosmochim. Acta 73 (4), 1039–1051.

Hermann, J., Green, D.H., 2001. Experimental constraints on high pressure melting in subducted crust. Earth Planet. Sci. Lett. 188, 149–186.

Hillier, S., 2003. Quantitative analysis of clay and other minerals in sandstones by X-ray powder diffraction (XRPD). In: Worden, R., Morad, S. (Eds.), Clay Mineral Cements in Sandstones. International Association of Sedimentologist, Special Publication. Blackwell Science, Oxford International, pp. 213–251.

Hofmann, A.W., 1988. Chemical differentiation of the Earth: the relationship between mantle, continental crust and oceanic crust. Earth Planet. Sci. Lett. 90, 297–314.

Hokada, T., 2001. Feldspar thermometry in ultrahigh-temperature metamorphic rocks: evidence of crustal metamorphism attaining ~1100°C in the Archean Napier Complex, East Antarctica. Am. Mineral. 86, 932–938.

Hoskin, P.W.O., 2005. Trace-element composition of hydrothermal zircon and the alteration of Hadean zircon from the Jack Hills, Australia. Geochim. Cosmochim. Acta 69, 637–648.

Hoskin, P.W.O., & Schaltegger, U., 2003. The composition of zircon and igneous and metamorphic petrogenesis. In: (Hanchar, J.M., & Hoskin, P.W.O., Eds.). "Zircon". Reviews in Mineralogy and Geochemistry. Vol. 53, Chapter 2, 27-62.

Imayama, T., Oh, C.-W., Baltybaev, S.K., Park, C.-S., Yi, K., Jung, H., 2017. Paleoproterozoic high-pressure metamorphic history of the Salma eclogite on the Kola Peninsula, Russia. Lithosphere 9 (6), 855–873. https://doi.org/10.1130/L657.1.

Johnson, M.C., Plank, T., 1999. Dehydration and melting experiments constrain the fate of subducted sediments. Geochem. Geophys. Geosyst. 1, 1999GC000014.

Jung, I., Schreyer, W., 2002. Synthesis, properties and stability of end member boromuscovite, KAl2[BSi3O10](OH)2. Contrib. Miner. Petrol. 143, 684–693.

Kaczmarek, M.-A., Müntener, O., Rubatto, D., 2008. Trace element chemistry and U-Pb dating of zircons from oceanic gabbros and their relationship with whole rock composition (Lanzo, Italian Alps). Contrib. Miner. Petrol. 155 (3), 295–312. https://doi.org/10.1007/s00410-007-0243-3.

Kaulina, T.V., 2010. Formation and Recrystallization of Zircons in Polimetamorphic Complexes. Kola SC RAS, Apatity, 144 p. (in Russian).

Kaulina, T.V., Yapaskurt, V.O., Presnyakov, S.L., Savchenko, E.E., Simakin, S.G., 2010. Metamorphic evolution of the Archean eclogite-like rocks of the Shirokaya and Uzkaya Salma area (Kola Peninsula): Geochemical features of zircon, composition of inclusions, and age. Geochem. Int. 48 (9), 871–890. https://doi.org/10.1134/S001670291009003X.

Kelsey, D.E., 2008. On ultrahigh-temperature crustal metamorphism. Gondwana Res. 13, 1–29.

Konilov, A.N., Shchipansky, A.A., Mints, M.V., Dokukina, K.A., Kaulina, T.V., Bayanova, T.B., Natapov, L.M., Belousova, E.A., Griffin, W.L., & O'Reilly, S.Y., 2011. The Salma eclogites of the Belomorian Province, Russia: HP/UHP metamorphism through the subduction of Mesoarchean oceanic crust. In: Ultrahigh-Pressure Metamorphism. 5 Years After the Discovery of Coesite and Diamond (eds Dobrzhinetskaya, L.F., Faryad, S.W., & Wallis, S.), pp. 623–670. Elsevier.

Korhonen, F.J., Stout, J.H., 2005. Undeformed kyanite- and borosilicate-bearing veins from the Grenville Province of Labrador: Evidence for rapid uplift. J. Metamorph. Geol. 23, 297–312.

Krogh, T.E., 1973. A low-contamination method for hydrothermal decomposition of zircon and extraction of U and Pb for isotopic age determinations. Geochim. Cosmochim. Acta 37 (3), 485–494.

Li, X., Zhang, L., Wei, C., & Slabunov, A.I., 2015. Metamorphic PT path and zircon U-Pb dating of Archean eclogite association in Gridino complex, Belomorian province, Russia. Precambrian Research, 268, 74-96. doi.org/10.1016/j.precamres.2015.07.009.

Li, X.L., Zhang, L.F., Wei, C.J., Slabunov, A.I., Bader, T., 2017a. Neoarchean Paleoproterozoic granulite-facies metamorphism in Uzkaya Salma eclogite-bearing mélange, Belomorian Province (Russia). Precambr. Res. 294, 257–283.

Li, X., Zhang, L., Wei, C., Slabunov, A.I., Bader, T., 2017b. Quartz and orthopyroxene exsolution lamellae in clinopyroxene and the metamorphic P-T path of Belomorian eclogites. J. Metamorph. Geol. 36 (1), 1–22. https://doi.org/10.1111/jmg.12280.

Lindsley, D.H., Nekvasil, H., 1989. A ternary feldspar model for all reasons. Eos 70, 506.

Liu, F., Zhang, L., Li, X., Slabunov, A.I., Wei, C., Bader, T., 2017. The metamorphic evolution of Paleoproterozoic eclogites in Kuru-Vaara, northern Belomorian Province, Russia: Constrains from P-T pseudosections and zircon dating. Precambr. Res. 289, 31–47. https://doi.org/10.1016/j.precamres.2016.11.011.

Ludwig, K.R., 1999. User's Manual for Isoplot/Ex, version 2.05: A Geochronological Toolkit for Microsoft Excel. Berkeley Geochronol. Center Spec. Publ. 1a. Berkeley, Cal.

Ludwig, K.R., 2000. SQUID 1.00. A User's Manual. Berkeley Geochronol. Center Spec. Publ. 2. Berkeley, Cal.

Mänttäri, I., Hölttä, P., 2002. U-Pb dating of zircons and monazites from Archean granulites in Varpaisjärvi, central Finland: Evidence for multiple metamorphism and Neoarchean terrain accretion. Precambr. Res. 118, 101–131. https://doi.org/10.1016/S0301-9268(02)00094-3.

Martin, A.J., 2000. Flaser and wavy bedding in ephemeral streams: a modern and an ancient example. Sed. Geol. 136 (1–2), 1–5.

Mints, M.V., Belousova, E.A., Konilov, A.N., Natapov, L.M., Shchipansky, A.A., Griffin, W.L., O'Reilly, S.Y., Dokukina, & K.A., Kaulina, T.V., 2010. Mesoarchean subduction processes: 2.87 Ga eclogites from the Kola Peninsula, Russia. Geology, 38 (8), 739–742.

Mints, M.V., Dokukina, K.A., 2020a. Age of eclogites formed by the subduction of the Mesoarchaean oceanic crust (Salma, Belomorian Eclogite Province, eastern Fennoscandian Shield, Russia): A synthesis. Precambr. Res. 350 https://doi.org/10.1016/j.precamres.2020.105879.

Mints, M.V., Dokukina, K.A., 2020b. The Belomorian eclogite province (eastern Fennoscandian Shield, Russia): MesoNeoarhean or Late Paleoproterozoic? Geodynamics Tectonophysics 11 (1), 151–200. https://doi.org/10.5800/GT-2020-11-1-0469.

Mints, M.V., Dokukina, K.A., Konilov, A.N., 2014. The Meso-Neoarchean Belomorian eclogite province: Tectonic position and geodynamic evolution. Gondwana Res. 25, 561–584.

Mints, M.V., Dokukina, K.A., Konilov, A.N., Belousova, E.A., Dokukin, P.A., Kaulina, T. V., Natapov, L.M., & Van, K.V., 2015. Mesoarchean Kola-Karelia continent. In: East European Craton: Early Precambrian history and 3D models of deep crustal structure, (eds Condie K. & Harvey F. E.), Boulder, Colorado, Geological Society of America Special Paper Vol. 510, pp. 15-88.

Moore, D.M., Reynolds, R.C., 1997. X-Ray Diffraction and the Identification and Analysis of Clay Minerals, 2nd edition. Oxford University Press Inc, New York, p. 400.

Nasdala, L., Zhang, M., Kempe, U., Panczer, G., Gaft, M., Andrut, M., Plötze, M., 2003. Spectroscopic methods applied to zircon. Rev. Mineral. Geochem. 53 (1), 427–467.

Page, F.Z., Essene, E.J., Mukasa, S.B., 2003. Prograde and retrograde history of eclogites from the Eastern Blue Ridge, North Carolina, USA. J. Metamorph. Geol. 21, 685–698.

Pearce, J. A., Stern, R.J., Bloomer, S.H. & Fryer, P., 2005. Geochemical mapping of the Mariana arc-basin system: implications for the nature and distribution of subduction components. Geochemistry, Geophysics, Geosystems, 6, 2004GC000895.

Perchuk, A.L., Morgunova, A.A., 2014. Variable P-T paths and HP-UHP metamorphism in a Precambrian terrane, Gridino, Russia: Petrological evidence and geodynamic implications. Gondwana Res. 25, 614–629.

Plank, T., Langmuir, C.H., 1998. The chemical composition of subducting sediment and its consequences for the crust and mantle. Chem. Geol. 145 (3–4), 325–394.

Pozhilenko, V.I., 2013. To the problem of eclogites in the Ensky segment of the Belomorian compound terrane (northeast of the Fennoscandian shield). Materials XLV Tectonic Conference, 163–167, Moscow GEOS (in Russian).

Rubatto, D., 2002. Zircon trace element geochemistry: partitioning with garnet and the link between U-Pb ages and metamorphism. Chem. Geol. 184, 123–138.

Ryan, J.G., Langmuir, C.H., 1993. The systematics of boron abundances in young volcanic rocks. Geochim. Cosmochim. Acta 57, 1489–1498.

Sawyer, E.W., 2001. Melt segregation in the continental crust: distribution and movement of melt in anatectic rocks. J. Metamorph. Geol. 18, 291–309.

Sharkov, E.V., 2006. Formation of layered intrusions and associated mineralization: Moscow. Scientific World, 368 p. (in Russian).
Schreyer, W., Werding, G., 1997. High-pressure behaviour of selected boron minerals and the question of boron distribution between fluids and rocks. Lithos 41, 251–266.
Shchipansky, A.A., Khodorevskaya, L.I., Konilov, A.N., Slabunov, A.I., 2012a. Eclogites from the Belomorian Mobile Belt (Kola Peninsula): geology and petrology. Russ. Geol. Geophys. 53 (1), 1–21.
Shchipansky, A.A., Khodorevskaya, L.I., Slabunov, A.I., 2012b. The geochemistry and isotopic age of eclogites from the Belomorian Belt (Kola Peninsula): evidence for subducted Archean oceanic crust. Russ. Geol. Geophys. 53 (3), 262–280.
Shchipansky, A.A., Sidorov, M.Yu. & Pisarev, G.V., 2016. Deep subduction in the Early Precambrian: UHP eclogite diamond-bearing rocks of the north-western part of the Belomorian mobile belt of the Baltic Shield. Materials XLVIII Tectonic Conference "Tectonics, Geodynamics and ore genesis fold belts and platforms", 2, 323–328, Moscow GEOS (in Russian).
Skublov, S.G., Balashov, Y.A., Marin, Y.B., Berezin, A.V., Mel'nik, A.E., Paderin, I.P., 2010a. U-Pb age and geochemistry of zircons from Salma eclogites (Kuru-Vaara deposit, Belomorian Belt). Dokl. Earth Sci. 432 (2), 791–798.
Skublov, S.G., Berezin, A.V., Marin, Y.B., Rizvanova, N.G., Bogomolov, E.S., Sergeeva, N. A., Vasil'eva, I.M., Guseva, V.F., 2010b. Complex isotopic-geochemical (Sm–Nd, U-Pb) study of Salma eclogites. Dokl. Earth Sci. 434 (2), 1396–1400.
Skublov, S.G., Astaf'ev, B.Y., Marin, Y.B., Berezin, A.V., Mel'nik, A.E., Presnyakov, S.L., 2011a. New data on the age of eclogites from the Belomorian mobile belt at Gridino settlement area. Dokl. Earth Sci. 439 (2), 1163–1170.
Skublov, S.G., Berezin, A.V., Mel'nik, A.E., 2011b. Paleoproterozoic eclogites in the Salma area, northwestern Belomorian mobile belt: composition and isotopic geochronologic characteristics of minerals and metamorphic age. Petrology 19 (5), 470–495.
Skublov, S.G., Berezin, A.V., Berezhnaya, N.G., 2012. General relations in the trace-element composition of zircons from eclogites with implications for the age of eclogites in the Belomorian mobile belt. Petrology 20 (5), 427–449. https://doi.org/10.1134/S0869591112050062.
Slabunov, A.I., Lobach-Zhuchenko, S.B., Bibikova, E.V., Sorjonen-Ward, P., Balangansky, V.V., Volodichev, O.I., Shchipansky, A.A., Svetov, S.A., Chekulaev, V.P., Arestova, N. A., & Stepanov, V.S., 2006. The Archean nucleus of the Fennoscandian (Baltic) Shield. In: European Lithosphere Dynamics (eds Gee, D.G., & Stephenson, R.A.), Memoirs Geological Society London Vol. 32, pp. 627–644.
Slabunov, A.I., Korol', N.E., Berezhnaya, N.G., Volodichev, O.I., & Sibelev, O.S., 2011. Main stages of the mafic granulites formation, Onego complex, Karelian craton: Petrology and isotopic dating (SHRIMP-II) of zircons. In: Granulite and eclogite complexes in the Earth's history. Extended abstracts and field trips guide book. Petrozavodsk, p. 215–217 (in Russian).
Slabunov, A.I., Volodichev, O.I., Skublov, S.G., Berezin, A.V., 2011b. Main stages of the formation of Paleoproterozoic eclogitized gabbro-norite: Evidence from U-Pb (SHRIMP) dating of zircons and study of their genesis. Dokl. Earth Sci. 437, 396–400.
Stepanova, A., Stepanov, V., 2010. Palaeoproterozoic mafic dyke swarms of the Belomorian Province, eastern Fennoscandian Shield. Precambr. Res. 183, 602–616. https://doi.org/10.1016/j.precamres.2010.08.016.
Stepanova, A.V., Sal'nikova, E.B., Samsonov, A.V., Egorova, S.V., Larionova, Yu.O., Stepanov, V.S., 2015. The 2.31 Ga mafic dykes in the Karelian Craton, eastern Fennoscandian shield: U–Pb age, source characteristics and implications for continental break-up processes. Precambrian Research, 259, 43-57.
Stepanova, A.V., Samsonov, A.V., Sal'nikova, E.B., Puchtel, I.S., Larionova, Yu.O., Larionov, A.N., Stepanov, V.S., Shapovalov, Y.B., Egorova, S.V., 2014. Palaeoproterozoic continental MORB-type tholeiites in the Karelian Craton: petrology, geochronology, and tectonic setting. J. Petrol., 55 (9), 1719-1751. 10.1093/petrology/egu039.
Svetov, S.A., 2005. Archean Magmatic Systems of Ocean– Continent Transition Zone in the Eastern Fennoscandian Shield. Petrozavodsk, Russian Academy of Sciences, Karelia Science Center, 230 p. (in Russian).
Svetov, S.A., Medvedev, P.V., 2013. Chemically precipitated siliceous rocks of Mesoarchean age – a unique environment for preservation of the early life traces. Lithosphere 6, 3–13 (in Russian).
Svetov, S.A., Svetova, A.I., 2004. The REE Systematics of Upper Archean Sedimentary Assemblages in Central Karelia. Dokl. Earth Sci. 394 (1), 104–108.
Svetova, A.I., Svetov, S.A., Nazarova, T.N., 2008. Mesoarchean sedimentary ensembles in ophiolite-like complexes of the Central Karelian terrain. Geology Mineral Deposits Karelia 5, 100–111 (in Russian).
Sun, S.S., & McDonough, W.F., 1989. Chemical and isotopic systematics of oceanic basalts: implications for mantle composition and processes. In: (Saunders, A.D., Norry, M.J., Eds.). Magmatism in the Ocean Basins. Geological Society, London, Special Publications 42, pp. 313-345.
Thompson, A.B., 1982. Dehydration melting of pelitic rocks and the generation of H2O undersaturated granitic liquids. Am. J. Sci. 282, 1567–1595.
Vavra, G., Schmid, R., Gebauer, D., 1999. Internal morphology, habit and U-Th-Pb microanalysis of amphibolite-to-granulite facies zircons: geochronology of the Ivrea Zone (Southern Alps). Contrib. Miner. Petrol. 134, 380–404.
Vielzeuf, D., Holloway, J.R., 1988. Experimental determination of the fluid absent melting relations in the pelitic system. Contrib. Miner. Petrol. 98, 257–276.
Volodichev, O.I., Slabunov, A.I., Bibikova, E.V., Konilov, A.N., Kuzenko, T.I., 2004. Archean eclogites in the Belomorian mobile belt, Baltic Shield. Petrology 12 (6), 540–560.
Volodichev, O.I., Slabunov, A.I., Sibelev, O.S., Skublov, S.G., Kuzenko, T.I., 2012. Geochronology, mineral inclusions, and geochemistry of zircons in eclogitized gabbronorites in the Gridino area, Belomorian Province. Geochem. Int. 50 (8), 657–670.
Whitney, D.L., Evans, B.W., 2010. Abbreviations for names of rock-forming minerals. Am. Mineral. 95, 185–187.
Yu, H., Zhang, L., Wei, C., Li, X., Guo, J., Bader, T., Qi, Y., 2018. The metamorphic evolution of Salma-type eclogite in Russia: Constraints fromzircon/titanite dating and phase equilibria modeling. Precambr. Res. 326, 363–384. https://doi.org/10.1016/j.precamres.2018.01.019.